A pigment-deficient mosquito line with fluorescent salivary glands enables *in vivo* imaging of individual *Plasmodium* sporozoites

Dennis Klug[1,#], Katharina Arnold[1,2], Eric Marois[1] and Stéphanie A. Blandin[1]

[1]Université de Strasbourg, CNRS UPR9022, INSERM U1257, Institut de Biologie Moléculaire et Cellulaire, 67000 Strasbourg, France

[2]Current address: German Cancer Research Institute (DKFZ), 69120 Heidelberg, Germany

to whom correspondence should be addressed:
dklug@unistra.fr

Abstract

Plasmodium parasites are the causative agent of malaria, a major health burden in sub-Saharan Africa. A key step in the transmission process of *Plasmodium* is the colonization of the salivary glands of the female *Anopheles* mosquito by the parasite sporozoite stage. How sporozoites recognize and invade the salivary glands is still poorly understood. Here we generated salivary gland reporter lines in the African malaria mosquito *Anopheles coluzzii* using salivary gland-specific promoters of the genes encoding anopheline antiplatelet protein (AAPP), the triple functional domain protein (TRIO) and saglin (SAG). The observed expression pattern of the DsRed and roGFP2 fluorescent reporters revealed lobe-specific activity of these promoters within the salivary glands, restricted either to the distal lobes or the middle lobe. We characterized four mosquito lines (AAPP-DsRed, AAPP-roGFP2, TRIO-DsRed and SAG-EGFP) in terms of localization, expression strength and onset of expression, as well as potential influences of the expressed fluorescent reporters on the infection with *Plasmodium berghei* and salivary gland morphology. Furthermore, using crosses with a pigmentation deficient *yellow(-)* mosquito line, we demonstrate that our salivary gland reporter lines represent a valuable tool to study the process of salivary gland colonization by *Plasmodium* parasites in live mosquitoes.

Introduction

Vector borne diseases have been a major health burden in the history of mankind. An efficient way to counteract diseases transmitted by blood sucking arthropods is to prevent transmission itself by reducing the number of vectors in the environment or by preventing vectors from biting humans in risk areas. As a consequence of malaria control interventions, approximately 663 million clinical malaria cases could be averted between 2000 and 2015. The most effective measure turned out to be the use of insecticide treated bet nets which prevented an estimated 68% of cases (Bhatt *et al.*, 2015). Still, preventive measures are counteracted by the very effective transmission of vector borne pathogens, which hampers eradication approaches. This is especially true for the causative agent of malaria, a protist named *Plasmodium*, which evolved highly specific adaptations to ensure efficient transmission between mosquitoes and human.

After infection of the mosquito midgut through the uptake of a blood meal from an infected host, *Plasmodium* parasites form a cyst, called oocyst, below the basal lamina of the midgut epithelium where they undergo multiple rounds of DNA replication. Rapid cell division, called schizogony, then follows, leading to the generation of several thousand of sporozoites per oocyst. These cells are released from the cysts and travel from the midgut to the salivary glands and, after being deposited in the skin during a blood meal, traverse the dermis, enter blood capillaries and reach the human liver. The sporozoites' distinctive cell polarization and crescent shape, in combination with high motility, allows them to „drill" through tissues. In addition, sporozoites are highly deformable enabling passing through densely packed environments. An important feature of sporozoites is their long survival time, up to several weeks, in mosquito tissues (Mayne, 1922).

While it is believed that the invasion process of the salivary glands by sporozoites that have egressed from oocysts is rapid (~1-10 minutes), *in vivo* data supporting this assumption is lacking (Douglas *et al.*, 2015). Still, the time a sporozoite needs to reach and successfully invade the glands is an important parameter, because at this timepoint, a mosquito is considered infective to humans. Moreover, the very quick invasion of the salivary glands suggests that sporozoites have specific receptors that recognize ligands exposed on the gland surface. Up to date only two mosquito proteins, saglin and circumsporozoite protein (CSP) binding protein (CSPBP), have been described to support salivary gland invasion of sporozoites (Ghosh and Jacobs-Lorena, 2009; Wang *et al.*, 2013). Knockdown experiments of both proteins have shown that sporozoite numbers in the salivary glands are reduced

compared to controls, indicating a lower invasion rate. However, overexpression of saglin in the distal lobes of *Anopheles stephensi* did not lead to an increase in the number of salivary gland resident sporozoites, and immunofluorescence-staining using anti-saglin antibodies indicated that this protein is expressed in the middle lobe of each salivary gland (O'Brochta *et al.*, 2019). This observation is puzzling since sporozoites strongly prefer to invade the distal lobes, with sporozoite invasion of the smaller middle lobe being less prominent or even completely absent (Wells and Andrew, 2019). Thus, the relation between saglin and sporozoites may be more complex than a simple ligand-receptor interaction. Microscopic studies of infected glands revealed that sporozoites form large accumulations in organized „stacks" inside cavities of acinar cells. The astonishing degree of order of these structures raises the question whether sporozoites can recognize each other. Alternatively, specifically preferred invasion sites may lead to accumulations at these entry points. However, since receptor-ligand interactions between sporozoites and acinar cells are still undefined, no specific entry site has been identified thus far.

Proteins secreted in the saliva of blood-sucking arthropods have been a long-term focus of interest. Saliva proteins often possess vasodilating, anti-coagulating and anti-inflammatory properties which counteract host responses and enable efficient blood feeding (Ribeiro and Francischetti, 2003). One protein specifically found in *Anopheles gambiae* saliva is TRIO (triple functional domain protein) that shares low homology to *Drosophila melanogaster* TRIO (Francischetti *et al.*, 2002, Arcà *et al.*, 2005, Dragovic *et al.*, 2018). Interestingly TRIO expression increases in the presence of *P. berghei* sporozoites (Dragovic *et al.*, 2018). The anopheline antiplatelet protein (AAPP) has anti-thrombotic functions and prevents collagen-induced platelet aggregation (Yoshida *et al.*, 2008; Hayashi *et al.*, 2012). Consistently, transgenic co-expression of an AAPP-specific single chain antibody blocking AAPP function negatively affects blood feeding *in vivo* (Islam *et al.*, 2019). The region upstream of the *aapp* gene was the first promoter used to drive salivary gland-specific transgenes in the Asian malaria mosquito *Anopheles stephensi* (Yoshida and Watanabe, 2006). Here we compare the promoter activities of the regions upstream of the *aapp*, *trio* and *saglin* genes in African *Anopheles coluzzii* mosquitoes and we test potential applications of the generated reporter lines to investigate sporozoite migration.

100 # Results

101

102 **Generation of transgenic mosquito lines with salivary gland-specific reporter expression**
103 **and low pigmentation**

104 To generate salivary gland reporter lines, the 5' upstream sequences of *saglin* (AGAP000610),
105 *aapp* (AGAP009974) and *trio* (AGAP001374) were used to drive the expression of DsRed
106 and hGrx1-roGFP2 from transgenic constructs integrated in the X1 docking line (**Fig. 1A, Fig.**
107 **S1**) (Volohonsky *et al.*, 2015). The fluorescence reporter hGrx1-roGFP2 was chosen because
108 it bears the advantages of EGFP and enables the measurement of the oxidation level of the
109 intracellular glutathione pool by ratiometric quantification (Gutscher *et al.*, 2008). We used
110 the *aapp* promoter sequence from *Anopheles coluzzii* orthologous to the one used to drive
111 salivary gland-specific transgene expression in *Anopheles stephensi* (Yoshida and Watanabe,
112 2006). For both *saglin* and *trio*, we defined putative promoter regions according to the
113 genomic context. In addition, as the selected *saglin* promoter region was very short (220bp,
114 **Fig. S2**), we also used CRISPR/Cas9 to integrate a fluorescence cassette encoding EGFP into
115 the endogenous *saglin* locus, replacing the coding sequence, to study *saglin* promoter activity
116 in its native genomic context. For this, site directed knock-in mutagenesis was performed by
117 injecting a plasmid encoding three guide RNAs targeting *saglin* and carrying a repair template
118 marked with *3xP3*-EGFP into mosquito eggs from a line with germline-specific expression of
119 Cas9 (*vasa-Cas9*), generating a *sag(-)KI* line (**Fig. 1B, S3A**). To place the *EGFP* gene
120 directly under control of the *saglin* promoter, the *3xP3* promoter used to selected transgenic
121 mosquito larvae was flanked by lox sites to enable its excision by Cre recombination (**Fig.**
122 **S3E**, Material & Methods). Similarly, we generated a knockin (KI) into the *yellow* gene that
123 encodes a protein required for the synthesis of black pigments in insects (Hunt and Bridges,
124 1916; Wittkopp, True and Carroll, 2002). For this, we used a plasmid with guide RNAs
125 specific for *yellow* and corresponding homology arms flanking a fluorescence cassette
126 expressing EGFP surrounded by lox sites (**Fig. S3B**). Through crossing of salivary gland
127 reporter lines with low pigmented *yellow(-)KI* mosquitoes, we aimed to improve the
128 fluorescence signal of the expressed reporter and extend the range of applications, e.g. for *in*
129 *vivo* imaging. Genotyping by PCR confirmed the successful generation of the salivary gland
130 reporter lines *aapp-DsRed*, *aapp-hGrx1-roGFP2*, *trio-DsRed* and *sag-DsRed* (**Fig S1**) as well
131 as the mosquito lines *sag(-)KI* and *yellow(-)KI* (**Fig S3C,D**). Loss of the *3xP3* promoter in
132 *sag(-)EX* mosquitoes (mosquitoes lacking the *3xP3* promoter after *Cre* mediated excision)

133 was confirmed by PCR in the progeny of a cross between the *sag(-)KI* line and a mosquito
134 line expressing *Cre* recombinase in the germline (**Fig. S3E**) (Volohonsky *et al.*, 2015).
135
136 **Lobe-specific transcriptional activation by *sag*, *aapp* and *trio* promoter sequences**
137 Dissection of female salivary glands revealed a highly specific expression pattern of DsRed,
138 EGFP and hGrx1-roGFP2 driven by *sag, aapp* and *trio* promoter sequences inside salivary
139 glands (**Fig. 1C**). While no fluorescence was observed for DsRed driven by the cloned 5'
140 upstream sequence of the *saglin* gene in dissected salivary glands (**Fig. S3A**), promoter
141 activity was detected in the line where *EGFP* replaced the *saglin* gene (**Fig. 1C**), indicating
142 that essential transcriptional elements localize outside of the intergenic sequence between
143 *AGAP000609* and *AGAP000610* (*saglin*) (**Fig. S3B**). Interestingly, fluorescence signals in
144 glands of female *aapp-DsRed*, *aapp-hGrx1-roGFP2* mosquitoes were restricted to the distal
145 lobes, while female *trio-DsRed* and *sag(-)EX* mosquitoes displayed fluorescence exclusively
146 in the middle lobe (**Fig. 1C**). This difference became especially evident when crossing *aapp-*
147 *hGrx1-roGFP2* mosquitoes with *trio-DsRed* mosquitoes giving rise to a trans-heterozygous
148 offspring displaying hGrx1-roGFP2 expression in distal lobes combined with DsRed
149 expression in the middle lobe (**Fig. 1C**). Similarly, when crossing *aapp* and *trio* DsRed
150 reporter lines, the entire salivary gland was red fluorescent in the F1 progeny (**Fig. 1C**).
151 Expression of *trio-DsRed* and *aapp-DsRed* was so strong that the respective parts of the
152 salivary gland appeared pink colored even in brightfield microscopy (**Fig. 1C**). Of note,
153 fluorescent reporter expression in the salivary glands of *aapp-DsRed*, *aapp-hGrx1-roGFP2*
154 and *trio-DsRed* mosquito colonies was restricted to females while no fluorescence signal
155 could be observed in this organ in males (**Fig. S4A**). Imaging of *aapp-DsRedP*, *aapp-hGrx1-*
156 *roGFP2* and *trio-DsRed* pupae during development revealed no distinct fluorescence signal in
157 the head part where the salivary glands are located (**Fig. S4B**). Still, DsRed expression was
158 visible in the salivary glands of *aapp-DsRed* females that had been dissected directly after
159 emergence (**Fig. 2A**), indicating that the *aapp* promoter is already active in pharate adults. In
160 contrast, no DsRed expression was observed in the glands of freshly hatched *trio-DsRed*
161 females (**Fig. 2A**). To evaluate the expression profile over time we performed a time-course
162 experiment by dissecting and imaging salivary glands of *trio-DsRed* and *aapp-DsRed* females
163 every day. DsRed expression guided by *aapp* and *trio* promoters increases steadily until day 5
164 after hatching (**Fig. 2B**). The strongest increase in fluorescence in *aapp-DsRed* females was
165 observed from day three to four, and from day four to five in *trio-DsRed* females (**Fig. 2B**).
166 The increase in DsRed in the salivary glands of *aapp-DsRed* and *trio-DsRed* females could

167 also be followed in transmitted light based on the pink coloration of the distal lobes (**Fig.**
168 **S4C**). In *Anopheles stephensi,* AAPP expression was shown by qRT-PCR to be upregulated
169 upon blood feeding (Yoshida and Watanabe, 2006). We followed DsRed fluorescence levels
170 in the salivary glands of *aapp-DsRed* and *trio-DsRed* sibling mosquitoes that were fed on
171 blood or kept on sugar (**Fig. 2C**). Our results confirm that the *aapp* promoter is induced upon
172 ingestion of a blood meal while there was no difference between blood-fed and sugar-fed in
173 females expressing the *trio-DsRed* transgene.
174
175 **Subcellular localization of fluorescent reporters and impact on salivary gland**
176 **morphology**
177 During first microscopic examinations using low magnification, different intracellular
178 localizations of the fluorescent proteins DsRed, EGFP and hGrx1-roGFP2 were observed (**Fig.**
179 **1C**), which was confirmed by confocal microscopy. DsRed expressed in the salivary glands
180 of *aapp-DsRed* and *trio-DsRed* mosquitoes appeared spotty and localized in vesicles within
181 the cytoplasm of the acinar cells, while hGrx1-roGFP2 and EGFP expressed in the glands of
182 *aapp-hGrx1-roGFP2* and *sag(-)KI* mosquitoes displayed a cytoplasmic localization (**Fig. 3A**).
183 Due to the anatomy of the secretory cells, which form an inward cavity into which saliva is
184 secreted, the DsRed-positive vesicles localize mainly at the outer rim of the salivary gland. In
185 contrast, localization of hGrx1-roGFP2 and EGFP was homogenous in the cytoplasm and
186 appeared to be also nuclear (**Fig. 3A**). We also observed morphological alterations. While
187 salivary glands of *aapp-DsRed*, *trio-DsRed* and *sag(-)KI* females were indistinguishable from
188 wild type (*G3*), the apex of the distal lobes in *aapp-hGrx1-roGFP2* expressing salivary glands
189 appeared shrunken and we detected a strangulation between the apex and the remainder of the
190 lobe (**Fig. 3B,C**). Acinar cells in the apex of the lobes that displayed the highest expression
191 levels of hGrx1-roGFP2, appeared thinned and atrophied, and presented an inflation of the
192 salivary duct in the apex region (**Fig. 3A**).
193
194 **Natural variation of DsRed expression in *trio-DsRed* mosquitoes**
195 During the generation of the salivary gland reporter lines and their subsequent outcrossing we
196 observed that most L1 mosquito larvae carrying the *trio-DsRed* transgene displayed DsRed
197 expression in the eyes (**Fig. S5A**), which was absent in the two other reporter lines *aapp-*
198 *DsRed* and *aapp-hGrx1-roGFP2*. Interestingly, a few L4 stage larvae of the *trio-DsRed* line
199 even displayed strong ubiquitous DsRed expression (**Fig. S5A**). At the pupal stage, DsRed
200 expression was detected in the ocellus, an eye spot close to the main compound eye, the

201 antennae and/or throughout the body. The observed expression patterns were highly variable
202 and ranged from completely non-fluorescent pupae to pupae expressing DsRed in all three
203 tissues (**Fig. S4B, S6A**). In adult mosquitoes, DsRed expression was less distinct compared to
204 pupae although complete body fluorescence was occasionally observed in both males and
205 females, with the strongest expression of DsRed in the salivary glands of females and the
206 palps and antennae of males (**Fig. S5B**). Dissections of adult mosquitoes displaying whole
207 body fluorescence at the pupal stage revealed strong and sex-independent DsRed signals in
208 Malphigian tubules, an insect organ that performs functions similar to the vertebrate kidney
209 (**Fig. S5C**). Of note, fluorescence in tubules strictly correlated to the high pupal fluorescence
210 phenotype and was never observed in mosquitoes hatched from low fluorescent pupae (**Fig.**
211 **S5D**). We next investigated sex-specificity of each fluorescence pattern at the pupal stage and
212 inheritance of the high and low fluorescent *trio-DsRed* transgene. Non-fluorescent pupae were
213 always females, while fluorescent antennae were observed exclusively in male pupae (**Fig.**
214 **S6B**). In contrast, the presence of a fluorescent ocellus or body fluorescence was sex-
215 independent (**Fig. S6B**). Quantification of the observed expression pattern revealed that a
216 fluorescent ocellus, either alone or in combination with body fluorescence, was most
217 frequently observed (**Fig. S6C**). The ratio of pupae that displayed body fluorescence to those
218 that did not was close to 50% (**Fig S6C**). To follow the inheritance pattern of high and low
219 body fluorescence, pupae were separated according to their fluorescence phenotype and
220 intercrossed. Quantification of pupal DsRed expression in the F1 generation revealed a strong
221 enrichment for whole body fluorescence (~80%) if high pupal body fluorescence was selected
222 in the previous generation. In contrast, no pupae with high body fluorescence were observed
223 in the offspring of mosquitoes hatched from low fluorescent pupae (**Fig. S6D**). This result
224 indicates a form of Mendelian inheritance, with the locus conferring high body fluorescence
225 being dominant over that conferring low body fluorescence. To investigate this further, virgin
226 female pupae of the F1 generation displaying high pupal DsRed expression were crossed with
227 wild type males. Ten single female families were created which were all screened for pupal
228 body fluorescence. All families except family 8 displayed a 1:1 distribution for high and low
229 pupal body fluorescence (**Fig. S6E**). Family 8 displayed exclusively high pupal body
230 fluorescence, indicating that the founder female was homozygous for the locus conferring
231 high body fluorescence, while all other females were heterozygous for the „low“ and the
232 „high“ *trio-DsRed* loci. Notably, we detected high DsRed signals in the salivary glands of all
233 adult females in families 5, 6, 7, 8 and 10 (other families were not investigated), regardless of
234 whether individuals hatched from pupae displaying high or low body fluorescence.

235 Genotyping of females homozygous for low *trio-DsRed* or heterozygous for WT/high *trio-*
236 *DsRed* revealed integration of the transgene into the X1 locus as a single copy (**Fig. S7**).
237
238 **Impact of reporter expression on infection with *Plasmodium berghei***
239 To test if the expression of a fluorescent reporter in the salivary glands alters parasite
240 development in the mosquito, we infected the three reporter lines *trio-DsRed*, *aapp-DsRed*
241 and *aapp-hGrx1-roGFP2* as well as the parental line *G3* with the rodent malaria parasite
242 *Plasmodium berghei* line Δp230p-GFP that constitutively expresses EGFP at high levels in all
243 developmental stages (Manzoni *et al.*, 2015). Parasite counts observed in reporter lines varied
244 from 118 to 142 oocysts and were not significantly different from the control (121 oocysts)
245 (**Fig. 4A**). The average number of salivary gland sporozoites at day 17-18 after infection was
246 8.200 to 17.400 sporozoites per mosquito in salivary gland reporter lines vs 9.600 in *G3*
247 controls (**Fig. 4B**). An average of 10.000 sporozoites is what is usually observed in our
248 laboratory, while numbers can fluctuate from 5.000 to more than 20.000 sporozoites per
249 mosquito even in non-transgenic lines, indicating no significant difference between the *G3*
250 control and reporter lines. To normalize the counts of salivary gland sporozoites relative to
251 differences in oocyst numbers, we calculated the number of sporozoites that had successfully
252 invaded the salivary glands per oocyst. Again, no significant difference was detected between
253 reporter lines (86-146 sporozoites per oocyst) and *G3* control (133) mosquitoes (**Fig. 4C**).
254 These results indicate that fluorescence expression in the salivary glands does not affect
255 parasite development in mosquitoes or salivary gland infection with sporozoites.
256
257 **Salivary gland reporter lines as a tool to investigate sporozoite biology / invasion of the**
258 **salivary glands**
259 We next investigated whether our highly fluorescent salivary gland reporter lines could
260 facilitate *in vivo* imaging of *Plasmodium* development through the cuticle of a living
261 mosquito using the same *P. berghei* line *Δp230p-GFP* (**Fig. 5A**). This line is bright enough to
262 make parasites visible through the mosquito cuticle, allowing pre-sorting of infected
263 mosquitoes based on fluorescence in the mosquito midgut, the salivary glands or in the wing
264 joint, a localization where hemolymph sporozoites tend to accumulate. Still, light absorption
265 by the pigmented cuticle and light scattering by chitin generate signal losses reducing image
266 quality and resolution. To reduce light absorption, we crossed *aapp-DsRed* mosquitoes,
267 displaying highly fluorescent salivary glands without altered morphology, with *yellow(-)KI*
268 mosquitoes, a loss-of-function line with low cuticle pigmentation (**Fig. 5A**). Yellow is a

269 protein required for the synthesis of black pigments in insects, its absence renders the cuticle
270 pale and yellowish (Hunt and Bridges, 1916; Wittkopp, True and Carroll, 2002). As expected,
271 *yellow(-)-aapp-DsRed* mosquitoes displayed a low pigmented cuticle in combination with
272 highly fluorescent salivary glands (**Fig. 5B**). The decrease in pigmentation greatly increased
273 the observed GFP signal visible through the cuticle, notably in strongly pigmented areas that
274 appear almost black in WT mosquitoes (**Fig. 5C**). We next imaged mosquitoes infected with
275 *P. berghei Δp230p-GFP* between day 17 and day 20 after infection, when sporozoites have
276 already invaded the salivary glands. In addition, mosquitoes were pre-sorted for GFP
277 fluorescence in the salivary glands (**Fig. S8A**) as well as in the wing joint (not shown) to
278 confirm the presence of sporozoites. While pre-sorting, we observed that the salivary glands
279 in a subset of mosquitoes (less than 1 out of 5) localized very close to the cuticle **(Fig. S8B,C**).
280 To facilitate *in vivo* imaging, we further selected mosquitoes positive for sporozoites and with
281 cuticular localization of at least one salivary gland. Subsequently the legs of selected
282 mosquitoes were removed and mosquitoes were glued on a microscopy slide. To prevent
283 squeezing of mosquitoes, cover slips were prepared with small plasticine feet at each corner,
284 and fixed with nail polish to prevent shifting of the cover against the microscopy slide (**Fig.**
285 **S8D**). Confocal imaging enabled to visualize precisely single sporozoites through the cuticle
286 close to the salivary gland as well as subcellular structures, like the cavities of acinar cells, of
287 the gland itself (**Fig. 6A**). Live imaging revealed that a considerable number of sporozoites
288 persist in tissues close to the gland and sometimes perform active movement (**Fig. 6B,C,**
289 **Movies 1 and 2**). We also observed single sporozoites moving actively through tissues in a
290 back and forth gliding manner (**Fig. 6B**, **Movie 3**) or making contact with the salivary gland
291 although no invasion event could be monitored (**Fig, 6D**).
292

293 ## Discussion

294 Mosquito salivary glands have long interested entomologists, parasitologists, virologists and
295 microbiologists because they are a key organ in the transmission of vector borne diseases.
296 Still, the host-pathogen interactions that allow the specific recognition and colonization of this
297 organ by different pathogens has been understudied, probably in part because of the relative
298 difficulty to access and visualize these processes in comparison to midgut invasion. The
299 reporter lines we generated in this study represent valuable tools to circumvent some of these
300 issues: they allow (1) to easily visualize the glands, even in brightfield or DIC microscopy,

301 (2) to distinguish distal and middle lobes of the salivary glands, and (3) to image single
302 sporozoites in proximity to the salivary glands *in vivo*.
303 We used the promoters of three salivary gland genes, *aapp*, *trio* and *saglin*, to drive
304 fluorescent reporter expression in *A. coluzzii* mosquitoes. The different fluorescence patterns
305 obtained in the salivary glands of these lines show that the proteomes of middle and distal
306 lobes are diverse and most likely contribute different saliva components. In addition, the
307 variable fluorescence intensity in the distal lobes of both *aapp* lines (stronger towards the
308 apex) point towards an even more complex expression pattern along the lobe. Interestingly the
309 *trio* and the *saglin* promoters were only active in the middle lobe, which, for saglin, is
310 coherent with immunofluorescence studies performed in *A. stephensi* (O'Brochta *et al.*, 2019).
311 This observation is puzzling since both proteins have been shown to either influence salivary
312 gland colonization or transmission of *Plasmodium* sporozoites (Ghosh and Jacobs-Lorena,
313 2009; Dragovic *et al.*, 2018) while parasites prefer to invade the distal lobes (Wells and
314 Andrew, 2019) that lack activity of *saglin* and *trio* promoters. A possible explanation is that
315 the site of expression of both proteins is not the site where they interact with parasites.
316 The absence of reporter expression in mosquitoes expressing DsRed controlled by the *saglin*
317 5' upstream sequence is likely due to the shortness of the cloned promoter sequence. The
318 *saglin* gene localizes in the middle of an array of four genes believed to be salivary gland-
319 specific (Francischetti *et al.*, 2002) and separated by short intergenic regions (**Fig. S1**).
320 Regulatory sequences controlling transcription are likely located upstream and/or downstream
321 of this array and might be shared by all four genes.
322 Notably, the reporter lines display different subcellular localizations of hGrx1-roGFP2, EGFP
323 and DsRed. While all expressed fluorescence, proteins lack any targeting signal which could
324 explain a different localization, only hGrx1-roGFP2 and EGFP localized within the cytoplasm.
325 In contrast, DsRed displayed a vesicular pattern in both middle (*trio*) and distal lobes (*aapp*),
326 while DsRed driven by the *aapp* promoter in *A. stephensi* mosquitoes is cytoplasmic (Yoshida
327 and Watanabe, 2006). The difference in localization between DsRed and other fluorescent
328 reporters points to the presence of a cryptic trafficking signal in DsRed recognized by the
329 acinar cells of *A. coluzzii*. Indeed, although we did not investigate their nature, we also
330 observed the presence of vesicles in the salivary glands of wild type mosquitoes with similar
331 distribution and morphology and displaying weak red autofluorescence (**Fig. S3A**). DsRed
332 could potentially be trafficked to this or a similar compartment explaining its unique
333 localization. Differences in salivary gland morphology between *aapp-DsRed* and *aapp-*
334 *hGrx1-roGFP2* expressing mosquitoes are likely due to the expression of human

335 Glutaredoxin 1 (hGrx1) and not of roGFP2, a protein derived from EGFP with 2 amino acid
336 changes. Indeed, no change in morphology was detected in *sag(-)EX* mosquitoes expressing
337 EGFP alone in the middle lobe. Still, EGFP appeared less expressed in the *sag(-)EX*
338 compared to hGrx1-roGFP2 in *aapp-hGrx1-roGFP2* (**Fig. 1**) and we cannot exclude that the
339 acinar cells of the middle and distal lobes react differently to the expression of the respective
340 reporters or that the cells show different responses to roGFP2 and EGFP. Despite its influence
341 on cell morphology the salivary glands of hGrx1-roGFP2 expressing mosquitoes retained
342 their integrity even with high mosquito age and apoptosis of cells expressing the fluorescent
343 reporter was not observed.
344 We also report a surprisingly large panel of fluorescence patterns in mosquitoes expressing
345 the *trio-DsRed* transgene. The *trio* promoter activated transcription of DsRed in the salivary
346 glands of all females (but not in males), but also in ocelli, antennae and Malpighian tubules as
347 well as whole body in some but not all mosquitoes, independently of their sex and with a
348 strict correlation between strong DsRed expression in pupal body and adult Malpighian
349 tubules. The fact that *trio* expression was reported to be salivary gland-specific (Dragovic *et*
350 *al.*, 2018) suggests that the region we selected upstream of *trio* does not contain all regulatory
351 elements that control its natural expression, or that the genomic context of the X1 locus may
352 influence its expression. Up to date, the number of available promoters able to drive
353 ubiquitous expression of transgenes in *Anopheles* mosquitoes is limited (Adolfi *et al.*, 2018),
354 thus replacing DsRed in a selected highly fluorescent line could provide a new means to
355 ubiquitously express transgenes. By sorting and crossing according to the observed pupal
356 fluorescence phenotype, it was possible to separate alleles conferring high and low pupal
357 body fluorescence, which allowed the production of a colony enriched with the high pupal
358 fluorescence phenotype and a colony showing only low pupal body fluorescence, especially
359 in the ocelli. This observation pointed towards a genetically encoded difference which is
360 inherited in a Mendelian manner rather than a transient (epi)genetic modification. Genotyping
361 confirmed the presence of a single copy of the transgene in the X1 locus in all types of
362 mosquitoes. Since fluorescent ocelli, antennae and whole body expression were only observed
363 in the *trio-DsRed* population, we propose that the different DsRed expression patterns are
364 locus-specific effects caused by interactions between the selected *trio* promoter sequence and
365 regulatory elements within sequences flanking the transgene, or in trans. The transgene
366 integration into the X1 locus may also have occurred with slight alterations that could
367 influence DsRed expression or a subset of mosquitoes may have inherited a second copy of
368 the transgene integrated in a different locus causing different locus-specific expression effects.

369 However, DsRed positive ocelli and antennae were observed in both high and low
370 fluorescence populations, which is most likely explained by a variable DsRed expression
371 from the transgene inserted at X1. While the observed DsRed expression patterns in larvae
372 and pupae are helpful in the laboratory to select transgenic individuals it also urges caution in
373 interpreting results as it clearly shows that transcription is contextual.
374 Intravital imaging has revealed the dynamics of parasite development inside its vertebrate
375 host (Sturm *et al.*, 2006; Wang *et al.*, 2020). While optical windows in mice is a well
376 implemented method (De Niz *et al.*, 2019), *in vivo* imaging through the cuticle of insects is
377 scarcely performed, mostly because it is difficult to achieve good resolution by imaging
378 through the insect cuticle that scatters and absorbs light very efficiently. Recent studies have
379 explored the possibility to circumvent this issue through the application of clearing protocols
380 on infected mosquitoes to improve resolution and enable imaging through whole mosquitoes
381 (de Niz *et al.*, 2019; Mori, Hirai and Mita, 2019). However, while these improvements are
382 remarkable, imaging of cleared specimens only represents snapshots whereas mapping of
383 dynamic processes would be desired. Imaging of tissues *ex vivo* in combination with the use
384 of hemolymph-like media allows the observation of dynamic processes (Klug and
385 Frischknecht, 2017). Still, imaging *ex vivo* samples can only be performed for a limited
386 amount of time and artifacts due to the artificial tissue environment cannot be excluded. A
387 step forward towards intravital imaging was made recently by developing a protocol that
388 combines feeding of dyes relevant for imaging with blood feeding prior to sample preparation
389 (Trisnadi and Barillas-Mury, 2020). Due to the inflation of the mosquito abdomen directly
390 after feeding, cuticle plates open up and create temporary optical windows that can be
391 exploited for microscopy. Still, in this case, mosquitoes were decapitated and tightly flattened
392 between microscopy slide and cover slip, thus allowing for optimal imaging but maintaining
393 *in vivo* conditions only for a limited time. To demonstrate the use of the salivary gland
394 reporter lines for imaging purposes, we crossed *aapp-DsRed* mosquitoes with the low
395 pigmented mosquito line *yellow(-)KI* deficient for black pigment synthesis. In a subset of
396 mosquitoes, salivary glands localized very closely to the cuticle allowing the recognition of
397 subcellular structures. Combining brighter cuticle with cuticular positioning of the salivary
398 glands within the mosquito thorax was instrumental to achieve visualization of single
399 sporozoites through the cuticle and we were able to get an insight into sporozoite behaviour *in*
400 *vivo*. It is generally believed that sporozoites, after they have been released from the oocyst,
401 are passively transported to the salivary glands and engage in active motility only upon
402 contact with acinar cells (Douglas *et al.*, 2015). Our *in vivo* observations indicate that

403 sporozoites can perform active motility even when not in contact with the salivary gland
404 (**Movie 1**, **2 and 3**). Interestingly, a significant number of sporozoites appeared trapped in
405 close proximity to the gland. These sporozoite accumulations are already known from other
406 sites of the mosquito circulatory system (Hillyer, Barreau and Vernick, 2007). Thus
407 sporozoite localization in the salivary gland area, for example through the detection of GFP,
408 does not necessarily represent a measure for successfully invaded sporozoites (**Fig. 6A**).
409 Here we provide a proof of concept of *in vivo* salivary gland imaging, and we hope that the
410 method can be further improved to gain a better insight of the invasion of salivary glands by
411 sporozoites. The injection of fluorescent beads or dyes could be used as vitality measure to
412 monitor the heartbeat of the mosquito while, at the same time, highlighting contact areas with
413 hemolymph and salivary glands. Also we did not exhaust the repertoire of possible genetic
414 modifications to decrease pigmentation of the cuticle. Deletion of the gene*s tan* and *ebony*,
415 two enzymes which regulate the homeostasis of the pigment precursors dopamine and N-ß-
416 alanyldopamine, in combination with the deletion of *yellow* could potentially further decrease
417 cuticle pigmentation (Wittkopp, True and Carroll, 2002; True *et al.*, 2005). Another
418 possibility could be the overexpression of arylalkylamine-*N*-acetyltransferase, an enzyme
419 converting dopamine into the sclerotizing precursor molecule N-acetyldopamine, which was
420 shown to affect pigmentation in different insect species by enhancing the production of
421 colorless components of the cuticle (Osanai-Futahashi *et al.*, 2012). A key improvement for *in*
422 *vivo* imaging would be an increase in the number of mosquitoes displaying ideally positioned
423 salivary glands. Preliminary monitoring experiments showed that the position of the gland
424 does not significantly change over time in adult mosquitoes indicating that positioning occurs
425 during metamorphosis. Should salivary gland positioning be genetically determined, selective
426 breeding may help to improve the ratio of mosquitoes with cuticular salivary glands. Taken
427 together we hope that the transgenic lines developed in this study can contribute to improve *in*
428 *vivo* imaging and salivary gland dissections in *Anopheles* mosquitoes, and enable real-time
429 imaging of *Plasmodium* and other vector borne pathogens.
430

431 ## Materials & methods

432

433 **Animals**

434 Transgenesis was performed in the *Anopheles coluzzii* strain X1 (Volohonsky *et al.*, 2015) or
435 in a strain expressing Cas9 from the X1 locus under control of the *vasa* promoter

436 (transgenesis plasmid: Addgene # 173670) and introgressed into the *Ngousso* genetic
437 background. Wild type *Anopheles coluzzii* strains *Ngousso* and *G3* were used as controls.
438 CD1 mice purchased from Charles River or from our own colonies were used for both
439 mosquito maintenance through blood meals, and for parasite maintenance and mosquito
440 infections. For infections with rodent malaria parasites, we made use of the *Plasmodium*
441 *berghei* line *Δ p230p-GFP* derived from the wild type background *P. berghei ANKA*
442 (Manzoni *et al.*, 2015).
443
444 **Breeding of mosquitoes**
445 *Anopheles coluzzii* mosquitoes were kept in standard conditions (27°C, 75-80% humidity, 12-
446 hr/12-hr light/dark cycle). Larvae were hatched in pans of osmosed water and fed with
447 pulverized fish food (TetraMin, Melle, Germany). Adult mosquitoes were maintained on a
448 10% sucrose solution. To propagate colonies, four to seven day old mosquitoes were blood
449 fed for 10-15 minutes on anesthetized mice and allowed to lay eggs on wet filter paper 2-3
450 days later. For mosquito blood feeding, female CD-1 mice (> 35g) were anesthetized with a
451 mixture of Zoletil (42.5 mg/kg) and Rompun (8.5 mg/kg) in 0.9% NaCl solution.
452
453 **Construction of salivary gland reporter transgenes**
454 The 5'upstream sequences of *saglin* (primers DK059 and DK065), *aapp* (primers KA001 and
455 KA014) and *trio* (primers KA008 and KA009) were amplified from genomic DNA of *G3*
456 mosquitoes isolated with the Blood & Tissue Kit (Qiagen) as shown in **File S1**. DsRed
457 (primers KA007 and KA010 for *aapp/trio*; DK060 and DK061 for *saglin*) and hGrx1-roGFP2
458 (primers KA013 and KA004) were amplified from the plasmids pJET-DsRed-SV40 and
459 pDSAP_actin-hGrx1-roGFP2 (donated by Raquel Mela-Lopez). Primers are shown in **Table**
460 **S2**. PCR was performed using Phusion polymerase according to the manufacturer
461 recommendations (ThermoFisher Scientific) and subcloned in the pJET vector using the
462 CloneJET PCR Cloning Kit (ThermoFisher Scientific). The 5'upstream sequence of the
463 *saglin* gene was fused to the *DsRed* gene by a Phusion mediated assembly PCR (TerMaat *et*
464 *al.*, 2009) before cloning into pJET. After sequence verification, assembly blocks were fused
465 into the destination vector pDSAP (Volohonsky et al., 2015, Addgene # 62293) using
466 Goldengate cloning and generating pDSAP-aapp-DsRed, pDSAP-aapp-hGrx1-roGFP2,
467 pDSAP-trio-DsRed and pDSAP-saglin-DsRed.
468

469 **Construct cloning for site-directed mutagenesis into *yellow* and *saglin* genes**
470 For the design of guide RNAs (gRNAs), the coding sequence of *saglin* as well as the first
471 exon of the *yellow* gene were manually searched for PAMs (NGG), with N representing any
472 nucleotide. Candidate gRNA sequences were investigated for potential off-target effects using
473 http://www.rgenome.net/cas-designer/ (Cas-OFFinder) (Bae, Park and Kim, 2014). We
474 selected gRNAs starting with a G considering the transcription start from the U6 promoter
475 and differing by ≥3 nucleotides from putative off-target sequences in the *A. coluzzii* genome.
476 For each knockin construct, linkers encoding the protospacer motif of three gRNAs (**Table**
477 **S1**) were generated by annealing two primers ordered from IDT DNA and cloned using *BbsI*
478 into pKSB-sgRNA (Addgene #173671—3) vectors containing the U6 snRNA polymerase III
479 promoter (AGAP013557), the invariable sequence of a standard crRNA-tracerRNA fusion
480 (Jinek et al., 2012), and the RNA polIII TTTTT terminator. The three complete gRNAs
481 blocks were then assembled into a single pKSB-sgRNA destination plasmid by GoldenGate
482 cloning using different but matching *BsaI* overhangs. For the construction of repair templates,
483 regions of homology on the 5' side (*saglin*: primers KA23 and DK105; *yellow*: primers
484 DK023 and DK024) and on the 3' side (*saglin*: primers KA29 and KA30; *yellow*: primers
485 DK025 and DK026) of the region targeted by the gRNAs were amplified from *Ngousso*
486 genomic DNA and subcloned in the pJET vector, generating plasmids pJET-5'saglin, pJET-
487 5'yellow, pJET-3'saglin and pJET-3'yellow. After sequence validation, all building blocks
488 were fused in the correct order in the destination plasmid pENTR using GoldenGate assembly
489 together with a building block containing either the fluorescence cassette pKSB-
490 Lox3xP3Lox-EGFP or pKSB-Lox3xP3-EGFP-Lox, generating pENTR-Saglin;Lox3xP3Lox-
491 EGFP and pENTR-Yellow;Lox3xP3-EGFP-Lox. Primers are shown in **Table S2**.
492
493 **Transgenesis of *A. coluzzii***
494 All plasmids used for DNA injections were purified using Endofree kits (Qiagen). Freshly
495 laid eggs of the docking line X1 or the *vasa-Cas9* line were injected as described (Fuchs,
496 Nolan and Crisanti, 2013; Pondeville *et al.*, 2014; Volohonsky *et al.*, 2015). For ΦC31-
497 integrase mediated transgensis a mix of three plasmids (pDSAP-aapp-DsRed, pDSAP-aapp-
498 hGrx1-roGFP2 and pDSAP-trio-DsRed) (~160 ng/µL) and the integrase helper plasmid
499 carrying the Vasa2-ΦC31-Integrase gene (Addgene # 62299, ~200 ng/µL) diluted in 0.5x
500 phosphate buffered saline (0.1 mM NaHPO4 buffer, 5 mM KCl, pH 6.8) was injected into
501 approximately 500 embryos. The plasmid pDSAP-saglin-DsRed was injected in the same
502 way but into a different batch of eggs. For site-directed knock-in mediated by Cas9, the

503 plasmid solution (pENTR-Saglin;Lox3xP3Lox-EGFP or pENTR-Yellow;Lox3xP3Lox-
504 EGFP) (~200-300 ng/µL) was diluted in PBS supplemented with 1 µM Scr7 to inhibit non-
505 homologous end joining. Each construct was injected in a separate batch of approximately
506 500 eggs obtained from *vasa-Cas9* females.
507
508 **Salivary gland reporter lines *sag-DsRed, trio-DsRed, aapp-DsRed* and *aapp-hGrx1-***
509 ***roGFP2***
510 Following egg micro-injection, surviving pupae were sorted according to sex, hatched in
511 separate cages (G0 generation) and crossed with ~100 mosquitoes of the other sex from a
512 mosquito line expressing CFP from the X1 docking site that was used as a balancer of the
513 new, non-fluorescent but puromycin resistant transgenic insertions at the same locus. Neonate
514 larvae from this cross were treated with puromycin (0.05 mg/mL). G1 pupae were
515 subsequently sex sorted and crossed with CFP positive mosquitoes to expand the population.
516 Adult puromycin resistant G2 females were sorted according to the observed fluorescence
517 phenotype (DsRed or roGFP2) in their salivary glands, reflecting the expression of the *trio-*
518 *DsRed*, *aapp-DsRed* or *aapp-hGrx1-roGFP2* transgenes and crossed to CFP balancer males.
519 For *sag-DsRed* females, sorting was not necessary, as transgenesis was performed separately
520 by injection of the pDSAP-saglin-DsRed plasmid alone. Puromycin-resistant G3 larvae were
521 raised, intercrossed and the G4 offspring was sorted by COPAS (Marois et al., 2012) for the
522 absence of CFP to select lines homozygous for *sag-DsRed*, *trio-DsRed*, *aapp-DsRed* and
523 *aapp-hGrx1-roGFP2*. Lines were then raised without puromycin treatment. Single females of
524 all generated colonies were genotyped by PCR to monitor correct integration of the transgene
525 into the docking site (**Fig. S1A,B**). Successfully genotyped mosquito colonies were expanded
526 and used to perform experiments.
527
528 ***yellow(-)KI* and *sag(-)KI* lines**
529 Pupae obtained from plasmid injected eggs were sorted according to sex and crossed with 100
530 *Ngousso* wild type partners. G1 neonate larvae were screened for the expression of EGFP
531 using a Nikon SMZ18 fluorescence Stereomicroscope. Selected transgenic larvae were sex
532 sorted at the pupal stage and crossed with an excess of wild type partners. The G2 progenies
533 (from a single positive G1 female for *sag(-)KI* and from 10 positive individuals for *yellow(-*
534 *)KI*) were COPAS sorted to enrich for the integrated transgene and to remove the *vasa-Cas9*
535 transgene (marked with DsRed). The generated *sag(-)KI* colony was kept in equilibrium with
536 the wild type allele, while the *yellow(-)KI* colony was completely homozygotized for the

537 transgene by selecting for mosquitoes with a yellow body color. Homozygous *sag(-)KI*
538 mosquitoes were crossed with the C2S line expressing Cre in the germline (Volohonsky *et al.*,
539 2015) for Cre recombinase-mediated excision of the lox cassette to generate *sag(-)EX*
540 mosquitoes.
541
542 **Genotyping of mosquito lines**
543 Genotyping was performed on genomic DNA extracted from single mosquitoes of *aapp-*
544 *DsRed*, *aapp-hGrx1-roGFP2*, *trio-DsRed*, *sag(-)KI, sag(-)EX* and *yellow(-)KI* colonies.
545 Genotyping PCRs were performed using GoTaq Green Mastermix (Promega) (**Fig. S1B**),
546 Phusion polymerase (ThermoFisher Scientific) or the Phire Tissue Direct PCR Master Mix
547 (ThermoFisher Scientific) (**Fig. S2** and **S7**) according to manufacturer recommendations. See
548 **Table S2** for genotyping primers.
549
550 **Mosquito infection and evaluation of parasite numbers**
551 Parasites were maintained as frozen stocks at -80ºC or by passage between mice. For this,
552 blood was taken by heart puncture from a donor mouse with a parasitaemia of 3-5%, diluted
553 to 2.10^7 parasitized erythrocytes in 100 µL 0.9% NaCl that were injected intravenously into a
554 naïve mouse. Parasitemia was monitored via flow cytometry (Accuri C6, BD biosciences)
555 three days later. Mosquitoes were fed for 10-15 min on anesthetized mice with 2.5 – 3.5%
556 parasitemia. Blood fed females were sorted and kept on 10% sucrose at 21ºC and 50-70%
557 humidity. Midguts and salivary glands were dissected in PBS under a SZM-2 Zoom
558 Trinocular stereomicroscope (Optika). Images were acquired with the Nikon SMZ18
559 Stereomicroscope (without coverslip) or with a Zeiss LSM 780 confocal microscope (sealed
560 coverslip). To count oocysts, midguts were dissected 7-8 days post infection. Fluorescence
561 images of infected midguts were processed using the watershed segmentation plugin (Soille
562 and Vincent, 1990) and oocysts were subsequently counted using the „analyze
563 particles“ function implemented in Fiji (Schindelin *et al.*, 2012). To count salivary gland
564 sporozoites, salivary glands were collected in PBS 17-18 days post infection and ground with
565 a plastic pestle for one minute. The number of sporozoites was measured using a Neubauer
566 hemocytometer under a light microscope (Zeiss).
567
568
569

570 **Fluorescence imaging, fluorescence measurements and image analysis**

571 Samples imaged using the Nikon SMZ18 Stereomicroscope were usually acquired using the
572 respective fluorescence filter to visualize expression of DsRed or roGFP2/EGFP combined
573 with brightfield to visualize the whole specimen. Images were taken using a 63-fold
574 magnification objective (NA 1.4) on a Zeiss LSM 780 confocal microscope (**Fig. 3A**), a
575 Zeiss Axiovert 200 fluorescence microscope **(Fig. S2A**) or using an iPhone 6 for the mounted
576 mosquitoes prepared for microscopy in **Fig. S8D**. All other images as well as images used for
577 fluorescence measurements were acquired with a Nikon SMZ18 Stereomicroscope. For
578 fluorescence quantifications, images were acquired in the DsRed channel and settings were
579 kept the same for all experiments. For each salivary gland, only a single lobe was measured
580 by analyzing a square of 51×51 pixels covering the central part of the fluorescent area to
581 determine the mean fluorescence intensity. The image processing for all experiments was
582 performed with Fiji (Schindelin *et al.*, 2012).

583

584 ***In vivo* imaging**

585 For *in vivo* imaging experiments, infected *yellow(-)-aapp-DsRed* mosquitoes were pre-
586 screened between days 17 - 21 post infection for the presence of hemolymph sporozoites
587 (hinge of the wing, GFP fluorescence) and salivary gland sporozoites (salivary gland, GFP
588 fluorescence) as well as for cuticular positioning of the salivary gland (DsRed signal) (**Fig.**
589 **S8B**). After removing their legs, mosquitoes were glued on a microscopy slide using small
590 amounts of UV-light reactive glue (Bondic Pocket) and covered with a coverslip prepared
591 with plasticine feet at each corner to prevent a squeezing of the sample. Corners of the cover
592 slip were coated with nail polish to prevent sliding. Imaging was performed on a Zeiss LSM
593 780 confocal microscope with GaAsP detector and Metamorph acquisition software.

594

595 **Statistical analysis**

596 Statistical analysis was performed using GraphPad Prism 5.0 (GraphPad, San Diego, CA,
597 USA). Data sets were either tested with a one-way ANOVA or a Student's t test. A value of
598 $p<0.05$ was considered significant.

599

600 **Data availability**

601 All data have been made available within this manuscript. Transgenic mosquito lines as well
602 as plasmids are available upon request.

603

604 **Ethics statement**

605 Experiments were carried out in conformity with the 2010/63/EU directive of the European
606 Parliament on the protection of animals used for scientific purposes. Our animal care facility
607 received agreement #I-67-482-2 from the veterinary services of the département du Bas Rhin
608 (Direction Départementale de la Protection des Populations). The use of animals for this
609 project was authorized by the French ministry of higher education, research and innovation
610 under the number APAFIS#20562- 2019050313288887 v3. The generation and use of
611 transgenic lines (bacteria, mosquitoes, parasite) was authorized by the French ministry of
612 higher education, research and innovation under the number 3243.

613

614 **Funding**

615 This work was supported by the Laboratoire d'Excellence (LabEx) ParaFrap (grant LabEx
616 ParaFrap ANR-11-LABX-0024), by the Equipement d'Excellence (EquipEx) I2MC (grant
617 ANR-11-EQPX-0022), by the ERC Starting Grant Nº260918, and by funding from CNRS,
618 Inserm, and the University of Strasbourg. DK is funded by a DFG postdoctoral fellowship
619 (KL 3251/1-1).

620

621 **Acknowledgements**

622 We thank Amandine Gautier for help with rearing mosquitoes and technical assistance during
623 infections with *P. berghei*, Sarra Manai for help with experiments, Jean-Daniel Fauny for
624 assistance during microscopy and the whole mosquito immune responses (MIR) team for
625 assistance with mosquito breeding and pupae collection.

626

627 Authors contributions

628 DK designed and performed experiments, analyzed data, made figures and wrote the draft.
629 KA cloned constructs, performed initial experiments and analyzed data. EM performed
630 transgenesis of mosquitoes. SB edited the draft and helped with conceptualization of
631 experiments. All authors edited and approved the manuscript for publication.

632

633 Competing interests

634 The authors declare no competing interests.

References

Adolfi, A. *et al.* (2018) 'Multi-tissue GAL4-mediated gene expression in all Anopheles gambiae life stages using an endogenous polyubiquitin promoter', *Insect Biochemistry and Molecular Biology*. doi: 10.1016/j.ibmb.2018.03.005.

Bae, S., Park, J. and Kim, J. S. (2014) 'Cas-OFFinder: A fast and versatile algorithm that searches for potential off-target sites of Cas9 RNA-guided endonucleases', *Bioinformatics*. doi: 10.1093/bioinformatics/btu048.

Berghammer, A. J., Klingler, M. and Wimmer, E. A. (1999) 'A universal marker for transgenic insects', *Nature*. doi: 10.1038/46463.

Bhatt, S. *et al.* (2015) 'The effect of malaria control on Plasmodium falciparum in Africa between 2000 and 2015', *Nature*. doi: 10.1038/nature15535.

Douglas, R. G. *et al.* (2015) 'Active migration and passive transport of malaria parasites', *Trends in Parasitology*, pp. 357–362. doi: 10.1016/j.pt.2015.04.010.

Dragovic, S. M. *et al.* (2018) 'Immunization with AgTRIO, a Protein in Anopheles Saliva, Contributes to Protection against Plasmodium Infection in Mice', *Cell Host and Microbe*. doi: 10.1016/j.chom.2018.03.008.

Engler, C. and Marillonnet, S. (2014) 'Golden Gate cloning', *Methods in Molecular Biology*. doi: 10.1007/978-1-62703-764-8_9.

Francischetti, I. M. B. *et al.* (2002) 'Toward a catalog for the transcripts and proteins (sialome) from the salivary gland of the malaria vector Anopheles gambiae', *Journal of Experimental Biology*.

Fuchs, S., Nolan, T. and Crisanti, A. (2013) 'Mosquito transgenic technologies to reduce plasmodium transmission', *Methods in Molecular Biology*, 923, pp. 601–622. doi: 10.1007/978-1-62703-26-7_41.

Ghosh, A. K. and Jacobs-Lorena, M. (2009) 'Plasmodium sporozoite invasion of the mosquito salivary gland', *Curr Opin Microbiol*, 12. doi: 10.1016/j.mib.2009.06.010.

Gutscher, M. *et al.* (2008) 'Real-time imaging of the intracellular glutathione redox potential', *Nature Methods*. doi: 10.1038/nmeth.1212.

675 **Hayashi**, H. *et al.* (2012) 'Anopheline anti-platelet protein from a malaria
676 vector mosquito has anti-thrombotic effects in vivo without compromising
677 hemostasis', *Thrombosis Research*. doi: 10.1016/j.thromres.2011.09.015.
678
679 **Hillyer**, J. F., Barreau, C. and Vernick, K. D. (2007) 'Efficiency of salivary
680 gland invasion by malaria sporozoites is controlled by rapid sporozoite
681 destruction in the mosquito haemocoel', *International Journal for Parasitology*.
682 doi: 10.1016/j.ijpara.2006.12.007.
683
684 **Hunt**, T. M. and Bridges, C. B. (1916) *Sex Linked Inheritance in Drosophila*,
685 *Carnegie Institution of Washington*.
686
687 **Islam**, A. *et al.* (2019) 'Anopheline antiplatelet protein from mosquito saliva
688 regulates blood feeding behavior', *Scientific Reports*. doi: 10.1038/s41598-019-
689 39960-2.
690
691 **Klug**, D. and Frischknecht, F. (2017) 'Motility precedes egress of malaria
692 parasites from oocysts', *eLife*, 6.
693
694 **Lee**, J. H. *et al.* (1996) 'Sequential amplification of cloned DNA as tandem
695 multimers using class- IIS restriction enzymes', *Genetic Analysis -*
696 *Biomolecular Engineering*. doi: 10.1016/S1050-3862(96)00164-7.
697
698 **Manzoni**, G. *et al.* (2015) 'A rapid and robust selection procedure for
699 generating drug-selectable marker-free recombinant malaria parasites', *Scientific*
700 *Reports*, 4(1), p. 4760. doi: 10.1038/srep04760.
701
702 **Mayne**, B. (1922) 'How Long Does a Mosquito Retain Malaria Parasites?',
703 *Public Health Reports (1896-1970)*. doi: 10.2307/4576379.
704
705 **Mori**, T., Hirai, M. and Mita, T. (2019) 'See-through observation of malaria
706 parasite behaviors in the mosquito vector', *Scientific Reports*. doi:
707 10.1038/s41598-019-38529-3.
708
709 **Natarajan**, R. *et al.* (2001) 'Fluorescent Plasmodium berghei sporozoites and
710 pre-erythrocytic stages: A new tool to study mosquito and mammalian host
711 interactions with malaria parasites', *Cellular Microbiology*, 3(6), pp. 371–379.
712 doi: 10.1046/j.1462-5822.2001.00117.x.
713
714 **De Niz**, M. *et al.* (2019) '3D imaging of undissected optically cleared
715 Anopheles stephensi mosquitoes infected with Plasmodium parasites', *bioRxiv*.
716 doi: 10.1101/682054.
717

De Niz, M. *et al.* (2019) 'Intravital imaging of host–parasite interactions in skin and adipose tissues', *Cellular Microbiology*. doi: 10.1111/cmi.13023.

O'Brochta, D. A. *et al.* (2019) 'Is Saglin a mosquito salivary gland receptor for Plasmodium falciparum?', *Malaria Journal*. doi: 10.1186/s12936-018-2634-5.

Osanai-Futahashi, M. *et al.* (2012) 'A visible dominant marker for insect transgenesis', *Nature Communications*. doi: 10.1038/ncomms2312.

Pondeville, E. *et al.* (2014) 'Efficient ΦC31 integrase–mediated site-specific germline transformation of Anopheles gambiae', *Nature Protocols*, 9(7), pp. 1698–1712. doi: 10.1038/nprot.2014.117.

Ribeiro, J. M. C. and Francischetti, I. M. B. (2003) 'Role of Arthropod Saliva in Blood Feeding: Sialome and Post-Sialome Perspectives', *Annual Review of Entomology*. doi: 10.1146/annurev.ento.48.060402.102812.

Schindelin, J. *et al.* (2012) 'Fiji: an open-source platform for biological-image analysis', *Nature Methods*, 9(7), pp. 676–682. doi: 10.1038/nmeth.2019.

Soille, P. and Vincent, L. M. (1990) '<title>Determining watersheds in digital pictures via flooding simulations</title>', in *Visual Communications and Image Processing '90: Fifth in a Series*. doi: 10.1117/12.24211.

Sturm, A. *et al.* (2006) 'Manipulation of host hepatocytes by the malaria parasite for delivery into liver sinusoids.', *Science (New York, N.Y.)*, 313(5791), pp. 1287–1290. doi: 10.1126/science.1129720.

TerMaat, J. R. *et al.* (2009) 'Gene synthesis by integrated polymerase chain assembly and PCR amplification using a high-speed thermocycler', *Journal of Microbiological Methods*. doi: 10.1016/j.mimet.2009.09.015.

Trisnadi, N. and Barillas-Mury, C. (2020) ' Live In Vivo Imaging of Plasmodium Invasion of the Mosquito Midgut ', *mSphere*. doi: 10.1128/msphere.00692-20.

True, J. R. *et al.* (2005) 'Drosophila tan encodes a novel hydrolase required in pigmentation and vision.', *PLoS genetics*, 1(5). doi: 10.1371/journal.pgen.0010063.

Volohonsky, G. *et al.* (2015) 'Tools for Anopheles gambiae Transgenesis', *G3 (Bethesda); Genes|Genomes|Genetics*, 5(6), pp. 1151–1163. doi: 10.1534/g3.115.016808.

Wang, J. *et al.* (2013) 'Anopheles gambiae circumsporozoite protein--binding protein facilitates Plasmodium infection of mosquito salivary glands', *J Infect Dis*, 208. doi: 10.1093/infdis/jit284.

Wang, L. T. *et al.* (2020) 'A Potent Anti-Malarial Human Monoclonal Antibody Targets Circumsporozoite Protein Minor Repeats and Neutralizes Sporozoites in the Liver', *Immunity*. doi: 10.1016/j.immuni.2020.08.014.

Wells, M. B. and Andrew, D. J. (2019) 'Anopheles salivary gland architecture shapes plasmodium sporozoite availability for transmission', *mBio*. doi: 10.1128/mBio.01238-19.

Wittkopp, P. J., True, J. R. and Carroll, S. B. (2002) 'Reciprocal functions of the Drosophila Yellow and Ebony proteins in the development and evolution of pigment patterns', *Development*.

Yoshida, S. *et al.* (2008) 'Inhibition of collagen-induced platelet aggregation by anopheline antiplatelet protein, a saliva protein from a malaria vector mosquito', *Blood*. doi: 10.1182/blood-2007-06-097824.

Yoshida, S. and Watanabe, H. (2006) 'Robust salivary gland-specific transgene expression in Anopheles stephensi mosquito', *Insect Molecular Biology*. doi: 10.1111/j.1365-2583.2006.00645.x.

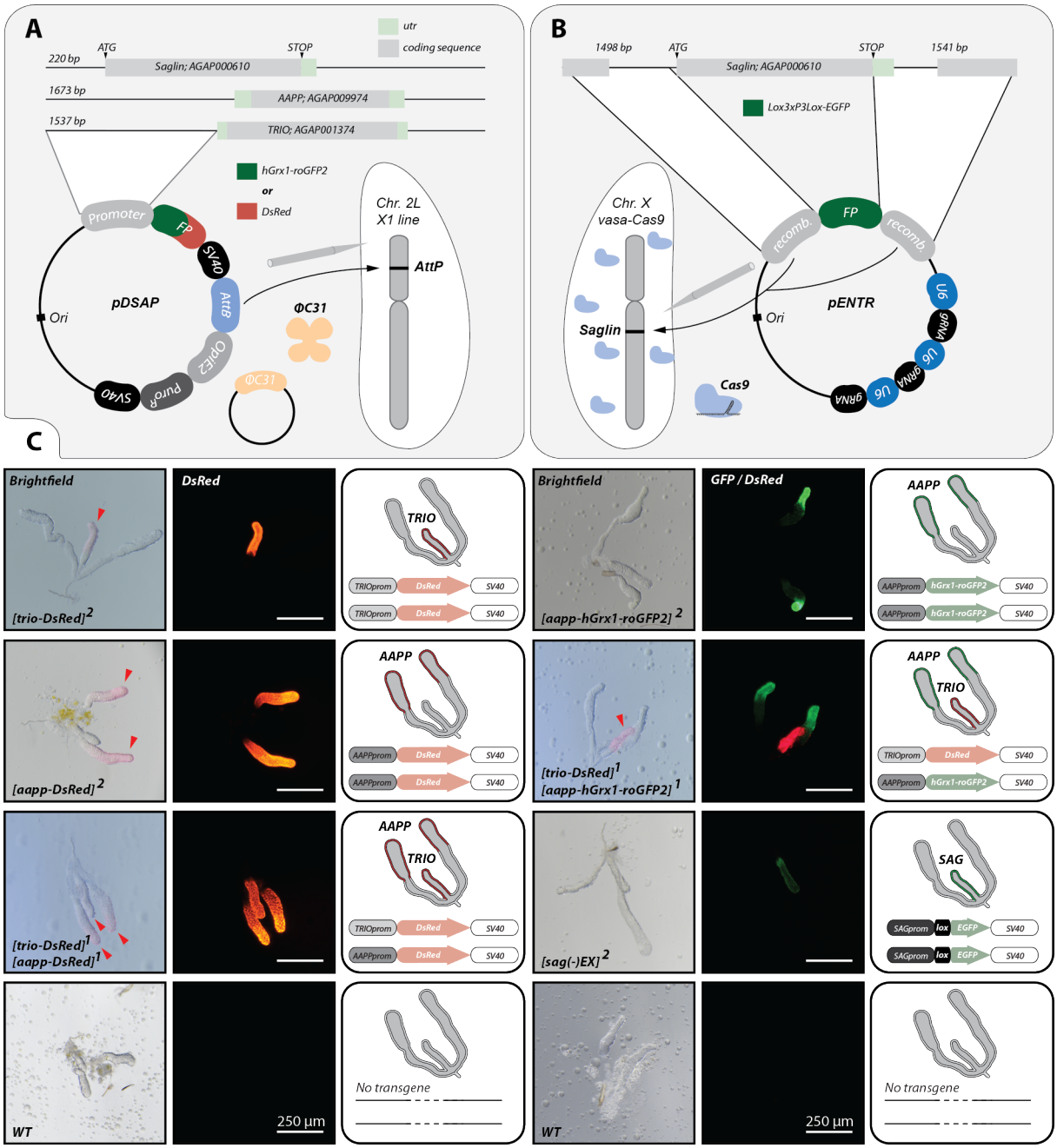

Figure 1. Lobe-specific reporter expression observed in female *aapp-DsRed*, *aapp-hGrx1-roGFP2*, *trio-DsRed* and *sag(-)EX* mosquitoes.
A) ΦC31 integrase-mediated transgene insertion. The *aapp*, *trio* and *saglin* promoter sequences were fused to *DsRed* or *hGrx1-roGFP2* within the pDSAP vector which enables chemical selection of mosquito larvae by puromycin. Transgenes were integrated by ΦC31 integrase-mediated recombination into the X1 line harbouring an *attP* site on chromosome 2L. **B)** Cas9-mediated knockin of a fluorescence cassette in the *saglin* gene (AGAP000610). Upstream and downstream sequences of *saglin* were cloned into the pENTR vector flanking a fluorescence cassette expressing EGFP under the control of the *3xP3* promoter. Three guides targeting *saglin* controlled by *U6* promoters were encoded on the same pENTR vector. Transgenesis was performed in mosquitoes with germline-specific expression of Cas9 (vasa-Cas9). **C)** Fluorescent reporter expression in *trio-DsRed*, *aapp-DsRed*, *aapp-hGrx1-roGFP2* and *sag(-)EX* expressing mosquito females in comparison to wild type (*G3*). Representative

800 images of salivary glands are shown in brightfield beside an image of the same gland in the
801 relevant fluorescence channel. Red arrows in brightfield images highlight the pink parts of
802 *aapp-DsRed* and *trio-DsRed* salivary glands in the absence of fluorescence excitation
803 indicating the high expression of DsRed. The illustration on the right of each panel indicates
804 the genotype of the gland as well as the observed fluorescence pattern. Scale bars: 250 µm.
805

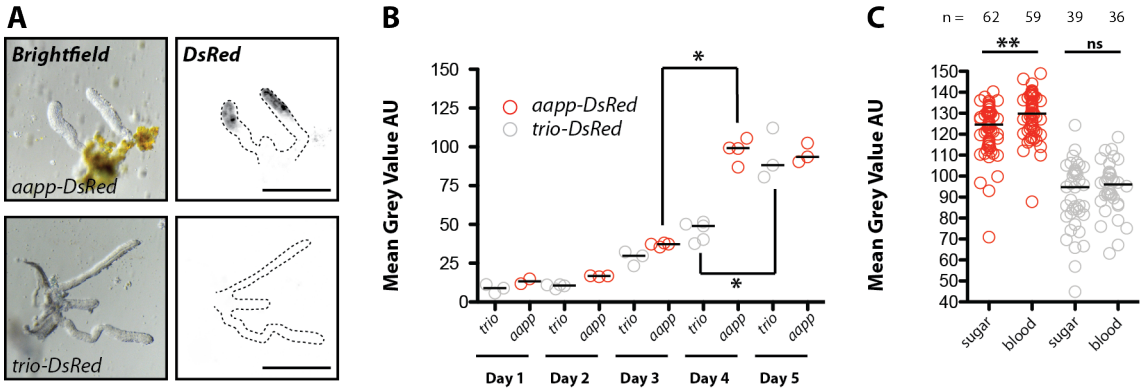

806
807
808 **Figure 2. Onset, strength and inducibility by blood feeding of reporter expression in**
809 ***aapp-DsRed* and *trio-DsRed* mosquitoes.**
810 **A)** Images of salivary glands dissected directly after mosquitoes emerged. DsRed expression
811 was observed in *aapp-DsRed* but not in *trio-DsRed* expressing salivary glands. Scale bar: 250
812 µm. **B)** Mean fluorescence intensity measurements of dissected *aapp-DsRed* and *trio-DsRed*
813 salivary glands from day one to day five after hatching. Data were normalized for the highest
814 exposure time. Each dot represents a single gland (2-5 glands / timepoint) and the bars, mean
815 values. *p<0.05, Mann Whitney test. **C)** The blood meal inducibility of the *trio* and the *aapp*
816 promoters was assessed by providing sibling females either with a blood meal or sugar
817 solution. Approximately 24h later, salivary glands were dissected, imaged and the mean
818 DsRed fluorescence intensity was quantified. Data pooled from three independent
819 experiments. Same representation and statistical analysis as in (B), **p=0.0015.
820

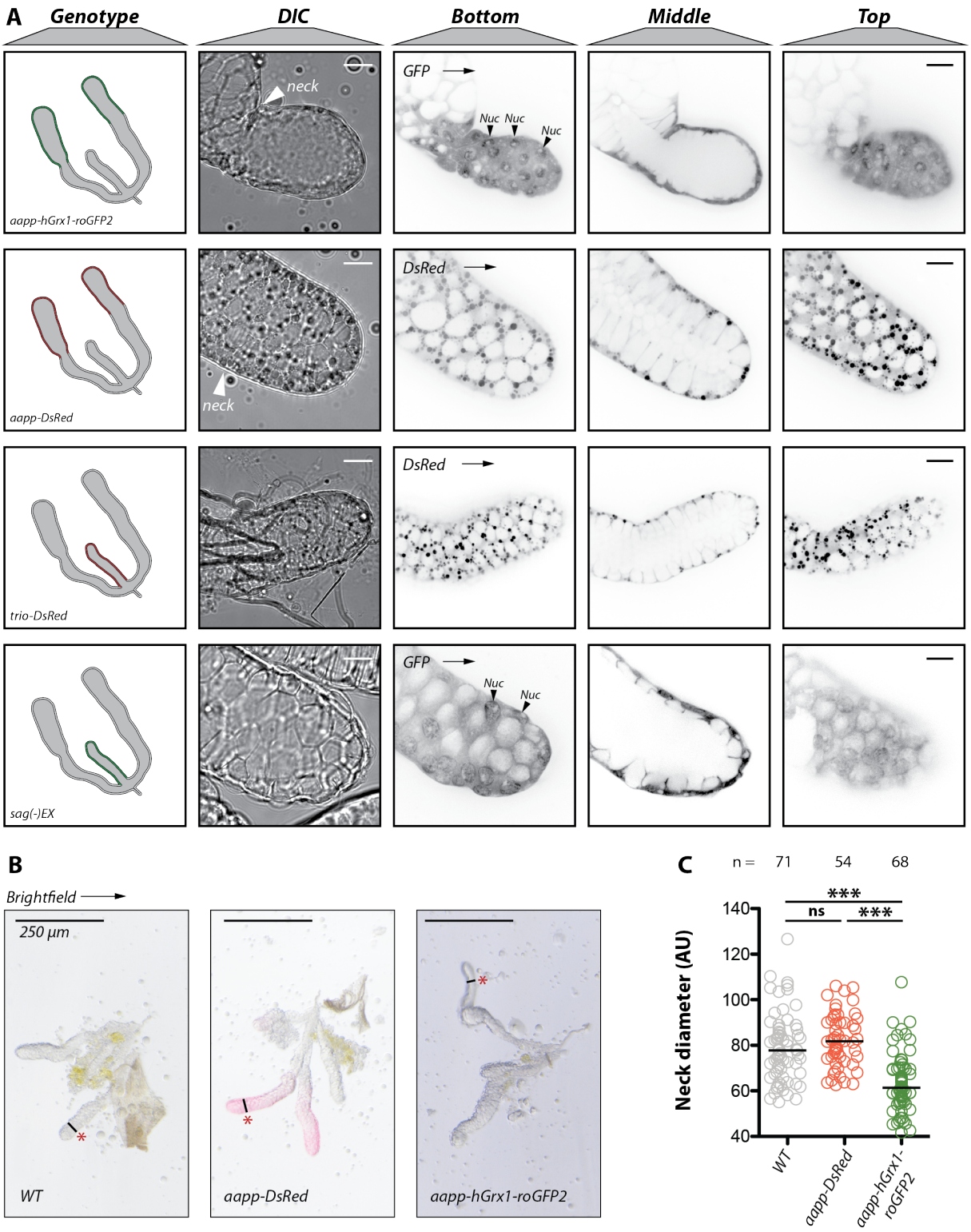

Figure 3. Different subcellular localizations of the expressed DsRed, EGFP and hGrx1-roGFP2 fluorescent reporters.

A) Differential interference contrast (DIC) and confocal fluorescence images of distal (*aapp-DsRed*, *trio-DsRed*) or middle (*trio-DsRed*, *sag(-)EX*) salivary gland lobes. Different z-sections (top, middle and bottom) of the same glands are displayed in the relevant fluorescence channel. The „neck“ regions of the *aapp-DsRed* and *aapp-hGrx1-roGFP2* expressing lobes are indicated by white arrows. Note that DIC and fluorescence images were

taken with a Hamamatsu Orca Flash 4.0 V1 and a Yokogawa CSU X-1 camera, respectively. Images between different channels are therefore not completely matching although depicting the same salivary gland. The illustration on the left depicts the genotype and corresponding expression pattern. Scale bars: 20 µm. **B)** Brightfield images of female wild type (*G3*), *aapp-DsRed* and *aapp-hGrx1-roGFP2* salivary glands. The „neck“ is indicated by a red asterisk and the measured diameter by a black line. Scale bars: 250 µm. **C)** Diameter measurements of the distal lobe neck region of *aapp-DsRed* and *aapp-hGrx1-roGFP2* in comparison to wild type (*G3*). The number of measurements is indicated above each genotype. Note that only the diameter of one distal lobe per gland was measured. Data represent ≥3 independent experiments. ***$p<0.0001$, one-way-ANOVA (Bonferroni's Multiple Comparison Test).

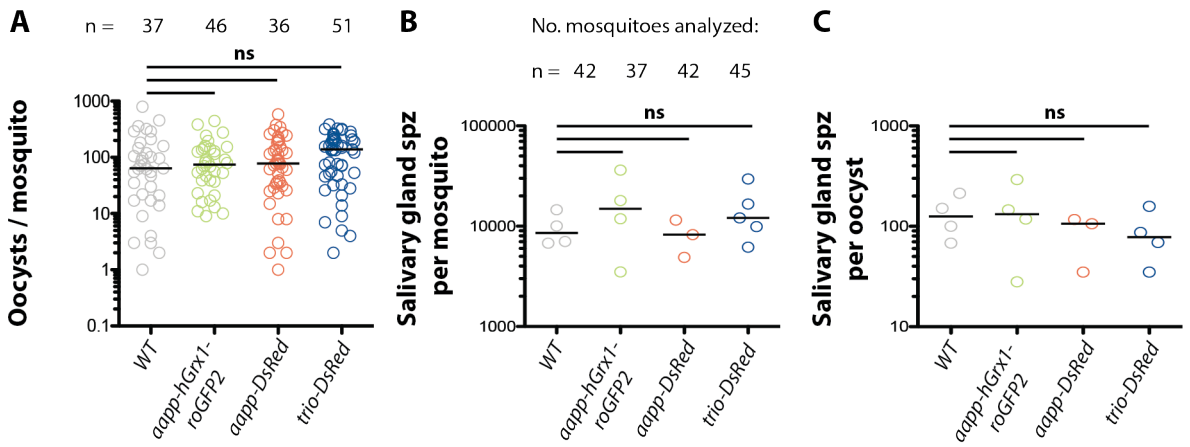

Figure 4. Oocyst densities and salivary gland colonization in *aapp-DsRed*, *aapp-hGrx1-roGFP2* and *trio-DsRed* mosquitoes infected with *P. berghei*.
Oocyst (**A**) and salivary gland sporozoite (spz) (**B**) counts in infected *aapp-DsRed*, *aapp-hGrx1-roGFP2* and *trio-DsRed* females in comparison to *wild type* (*G3*) females. Data pooled from three biological replicates. The total number of dissected mosquitoes is given above each genotype. **C)** Number of salivary gland sporozoites (spz) per oocyst for all three reporter lines in comparison to *wild type* (WT: *G3*). The invasion rate was calculated using the data shown in (A) and (B). Each dot represents a single mosquito (A) or the result of a counting (B and C), the median is indicated by a bar. All data were tested for significance using a one-way-ANOVA (Kruskal-Wallis test). ns: not significant (p>0.05).

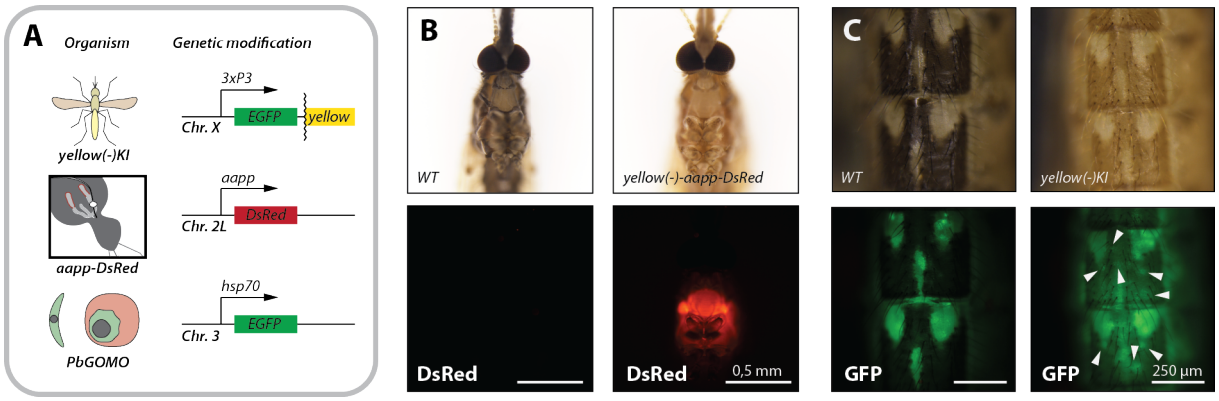

Figure 5. Salivary gland reporter lines as tool for *in vivo* imaging.
A) Genetic models used for *in vivo* imaging. Mosquitoes carrying the *aapp-DsRed* transgene were crossed with *yellow(-)KI* mosquitoes displaying reduced black pigmentation. Infections were carried out using the highly fluorescent *P. berghei* line *Δp230p-GFP* constitutively expressing EGFP (Manzoni *et al.*, 2015). **B)** Pigmentation phenotype and salivary gland-specific DsRed expression of *yellow(-)-aapp-DsRed* mosquitoes in comparison to wild type (WT: *Ngousso*). Brightfield and DsRed expression of the same field of view. Scale bar: 0.5 mm. **C**) Images of the abdomen of infected *yellow(-)KI* and wild type (*Ngousso*) mosquitoes. Brightfield and GFP expression of the same field of view. White arrows point towards oocysts visible through strong pigmented areas of the cuticle of *yellow(-)KI* mosquitoes. Scale bar: 250 µm.

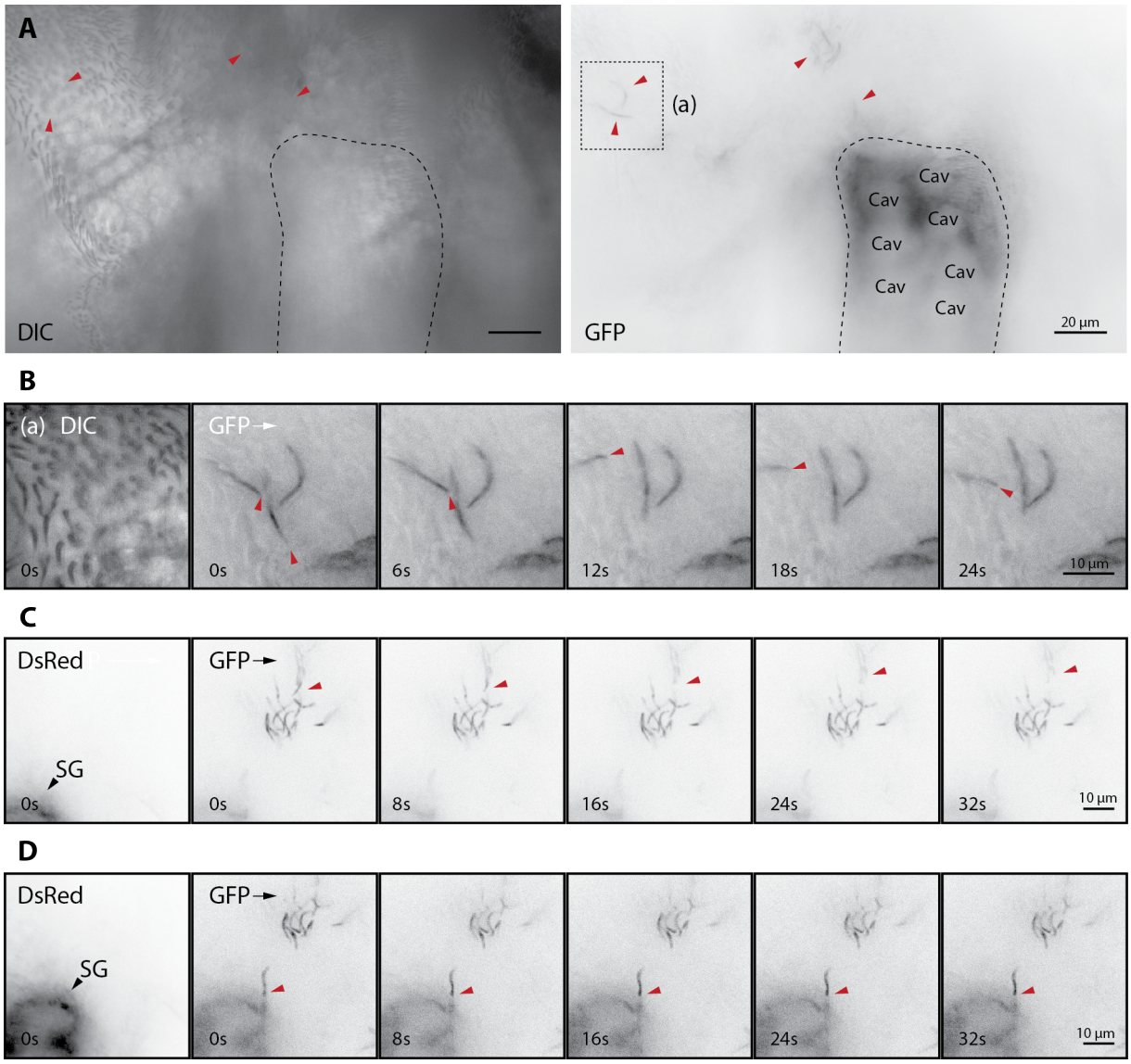

Figure 6. Confocal imaging of sporozoite salivary gland interactions in live mosquitoes. **A)** Thorax view of a *yellow(-)-aapp-DsRed* female mosquito infected with *P. berghei Δp230p-GFP*. Differential interference contrast (DIC) image on the left and the GFP signal on the right. Note that the DsRed expression in the salivary glands is strong enough to be visible in the GFP channel. Red arrows point towards sporozoites and the dashed line in the DIC image indicates the position of the salivary gland as seen in the GFP channel. Scale bar: 20 µm. **B)** Zoom on a group of sporozoites sequestered in close proximity to the salivary gland in the area boxed as (a) in the previous image (A). DIC image and a time series of the GFP signal with 6 s between frames. Red arrows point towards sporozoites displaying movement. Scale bar: 10 µm. **C,D)** Accumulation of sporozoites close to the salivary gland. **C** and **D** show the same salivary gland with altered focus and shifted field of view. DsRed signal (left) to indicate the position of the salivary gland (SG), and time series of the GFP signal with 8 s between frames. The red arrow points towards sporozoites displaying active movement (C) or towards a sporozoite in contact with the salivary gland (D). Scale bar: 10 µm. Note that imaging was performed with a Hamamatsu Orca Flash 4.0 V1 camera for A) and B) or a Yokogawa CSU X-1 for C) and D) using a 63-fold magnification objective (N.A. 1.4).

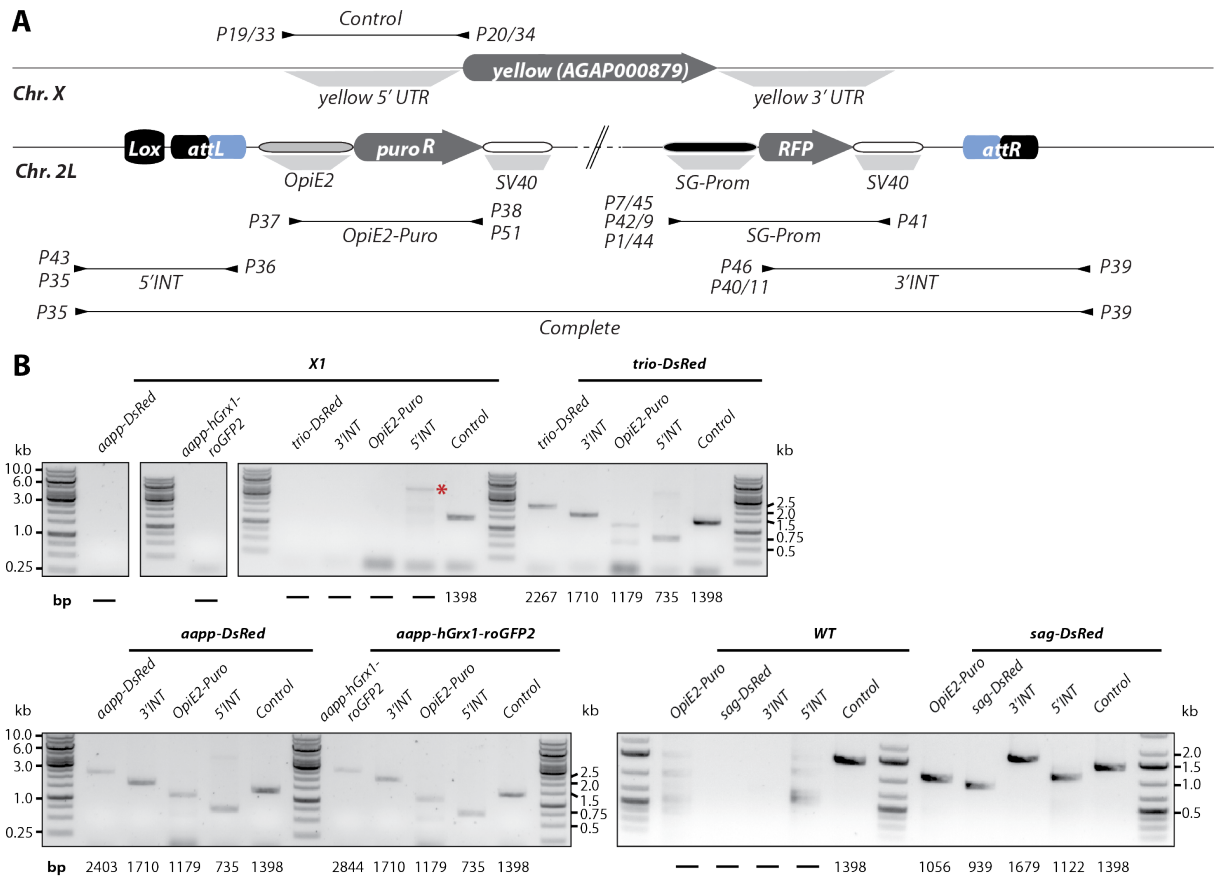

Figure S1. Genotyping of the salivary gland reporter lines *aapp-DsRed*, *aapp-hGrx1-roGFP2 and trio-DsRed*.

A) Schematic representation of salivary gland reporter transgenesis cassettes inserted on chromosome 2L. Fusion of *attB* and *attP* sites generate *attL* and *attR* sites after integration. The *Lox* site upstream of the transgene is a remnant of the fluorescence cassette initially required to select the docking line X1. Note that the illustration is not drawn to scale. **B)** Genotyping of generated transgenic mosquito colonies in comparison to *wild type* (WT: *G3*) or the parental line X1. Five different analytical PCRs were performed. The 5'INT and 3'INT PCRs amplify the integration borders upstream and downstream of the transgene, respectively. The presence of the puromycin resistance cassette was tested (OpiE2-Puro PCR). To ensure integration of the relevant fluorescence cassette, the PCRs aapp-DsRed, aapp-hGrx1-roGFP2, trio-DsRed and sag-DsRed were performed. In addition, a PCR control amplifying the 5'UTR of the *yellow* gene on chromosome X was included. Genotyping primers and amplified sequences are indicated with arrowheads and thin black lines in the scheme (A). The red asterisk marks an unspecific band only observed in the control X1.

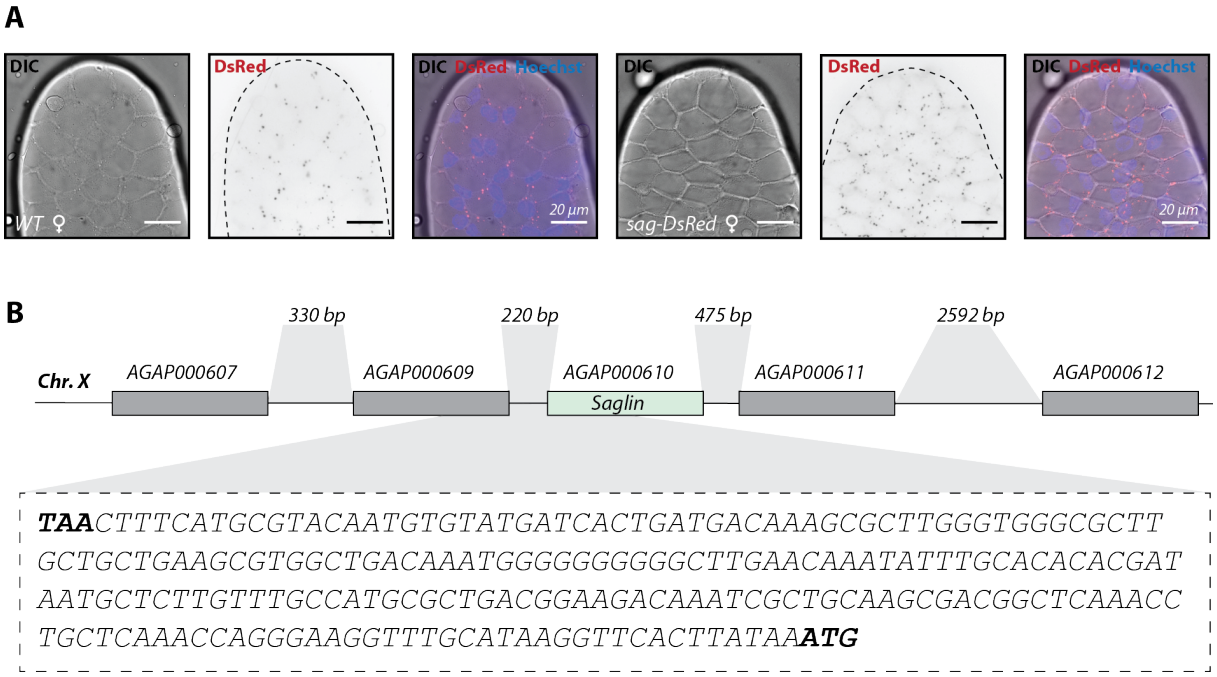

Figure S2. The intergenic sequence between AGAP000609 and AGAP000610 (*saglin*) displays no promoter activity.

A) Images of salivary glands from a *sag-DsRed* and a wild type female (*Ngousso*). Dissected glands were stained with Hoechst 33342 to detect the nuclei of acinar cells. The dotted black line in DsRed images indicates the outline of the salivary gland lobe observed in DIC. Scale bar: 20 µm. **B)** Genomic context of *saglin* (AGAP000610) with neighboring genes. The length of intergenic sequences is indicated above the scheme and the sequence tested for promoter activity located between AGAP000609 and *saglin* is shown. The stop codon TAA of AGAP000609 and the start codon of *saglin* are highlighted in black. The length of the cloned sequenced intergenic sequence was 220 bp (without stop codon of AGAP000609 and start codon of *saglin*). Note that the illustration is not drawn to scale.

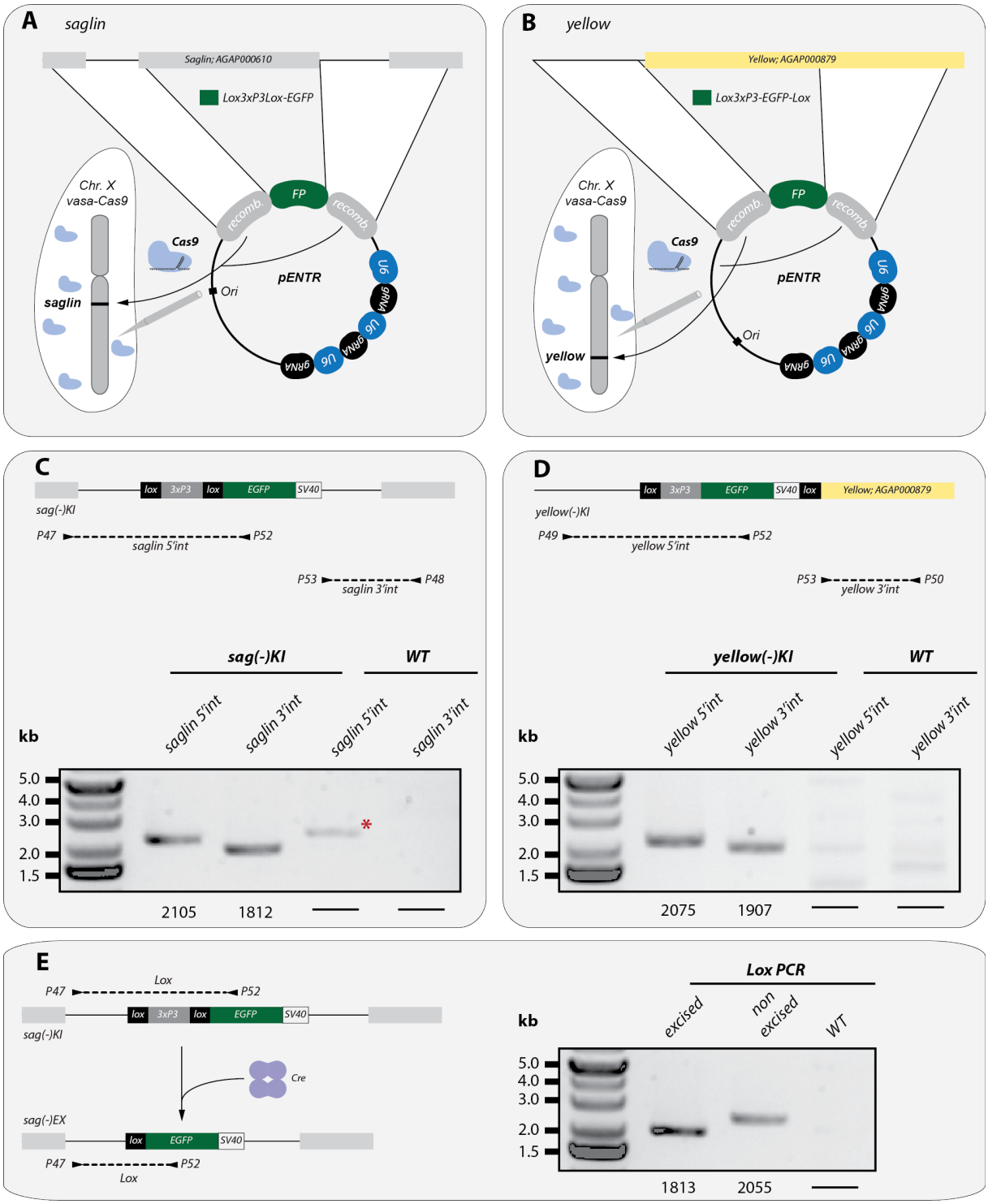

Figure S3. Genotyping of *sag(-)KI*, *sag(-)EX* and *yellow(-)KI* mosquitoes. *Sag(-)KI* (**A**) and *yellow(-)KI* (**B**) mosquitoes were generated by injecting embryos expressing Cas9 (*vasa-Cas9*) with plasmids carrying repair templates that contain a Lox3xP3Lox-EGFP or a Lox3xP3-EGFP-Lox cassette flanked with upstream and downstream sequences of the respective targeted locus, in combination with three guide RNAs specific for the *saglin* (AGAP000610) or *yellow* gene (AGAP000879). Genotyping of the 5' and 3' integration borders revealed successful integration of the transgenes into *saglin* (**C**) and *yellow* (**D**). The red asterisk marks an unspecific PCR product observed in the wild type control (WT: *Ngousso*). **E)** To investigate the native expression of the *saglin* promoter, the *3xP3* promoter

930 initially used to select transgenic *sag(-)KI* mosquito larvae was removed by Cre-mediated
931 excision. The loss of the *3xP3Lox* sequence in *sag(-)EX* mosquitoes was confirmed by PCR.
932

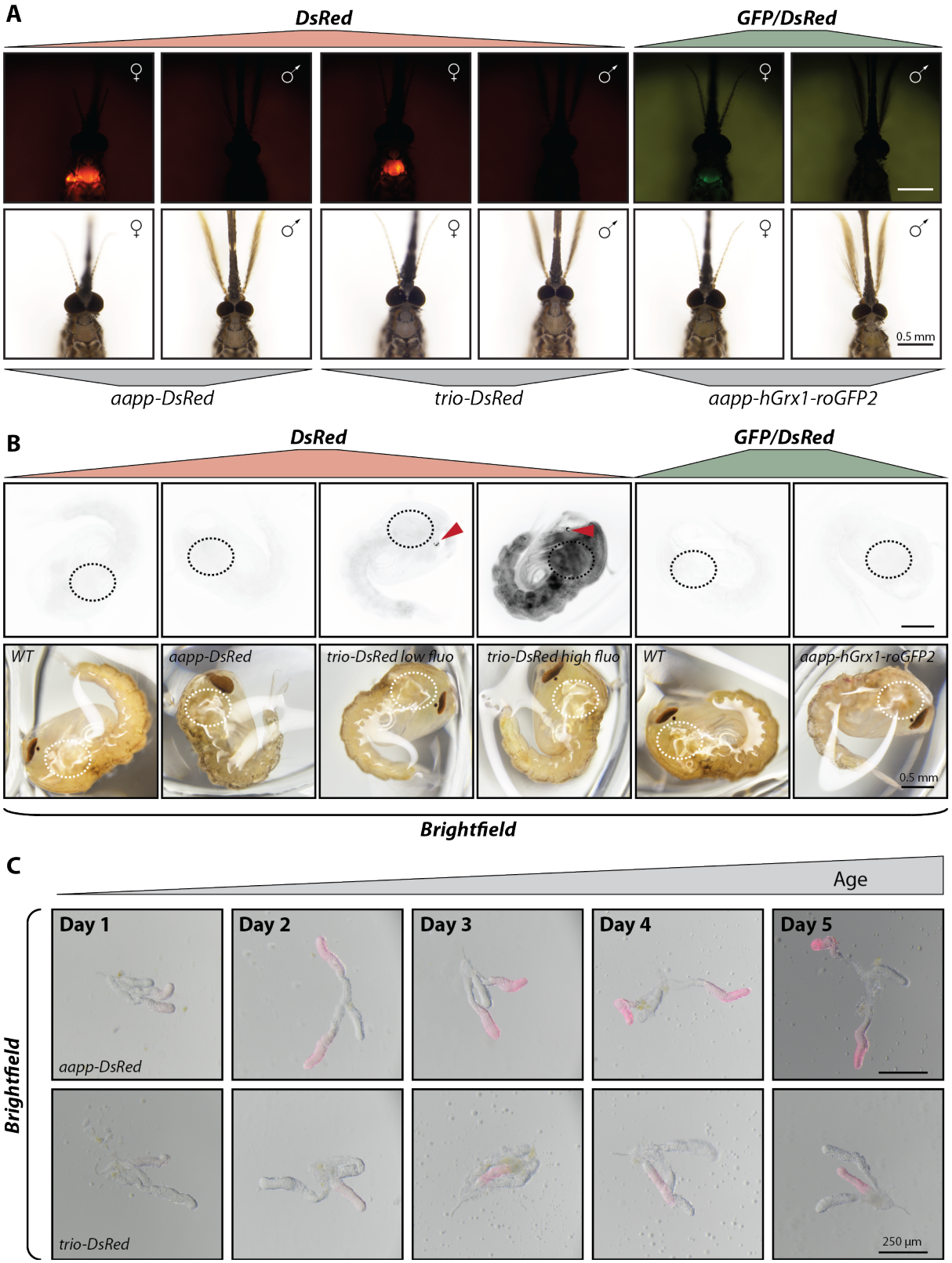

Figure S4. Expression driven by *trio* and *aapp* promoters is female- and adult-specific and the fluorescent reporter accumulates after the emergence of adults.
A) Fluorescence and brightfield images of female / male pairs of *trio-DsRed*, *aapp-DsRed* and *aapp-hGrx1-roGFP2* mosquitoes. Note that all depicted mosquitoes were bred in synchrony and were seven day old (+/- 1 day). Scale bar: 0.5 mm. **B)** Fluorescence and brightfield images of *aapp-DsRed*, *trio-DsRed* and *aapp-hGrx1-roGFP2* pupae in comparison

941 to *wild type* (*G3*). Dotted circles indicate the putative position of the salivary glands. *Trio-*
942 *DsRed* pupae with low and high DsRed body expression are shown for comparison. The red
943 arrows indicate DsRed positive ocelli observed in most *trio-DsRed* pupae. Scale bar: 0.5 mm.
944 **C)** Brightfield images of *aapp-DsRed* and *trio-DsRed* female salivary glands from day 1 to
945 day 5 after hatching (a single image per day and per line). All images were acquired using the
946 same settings. Scale bar: 250 µm.
947

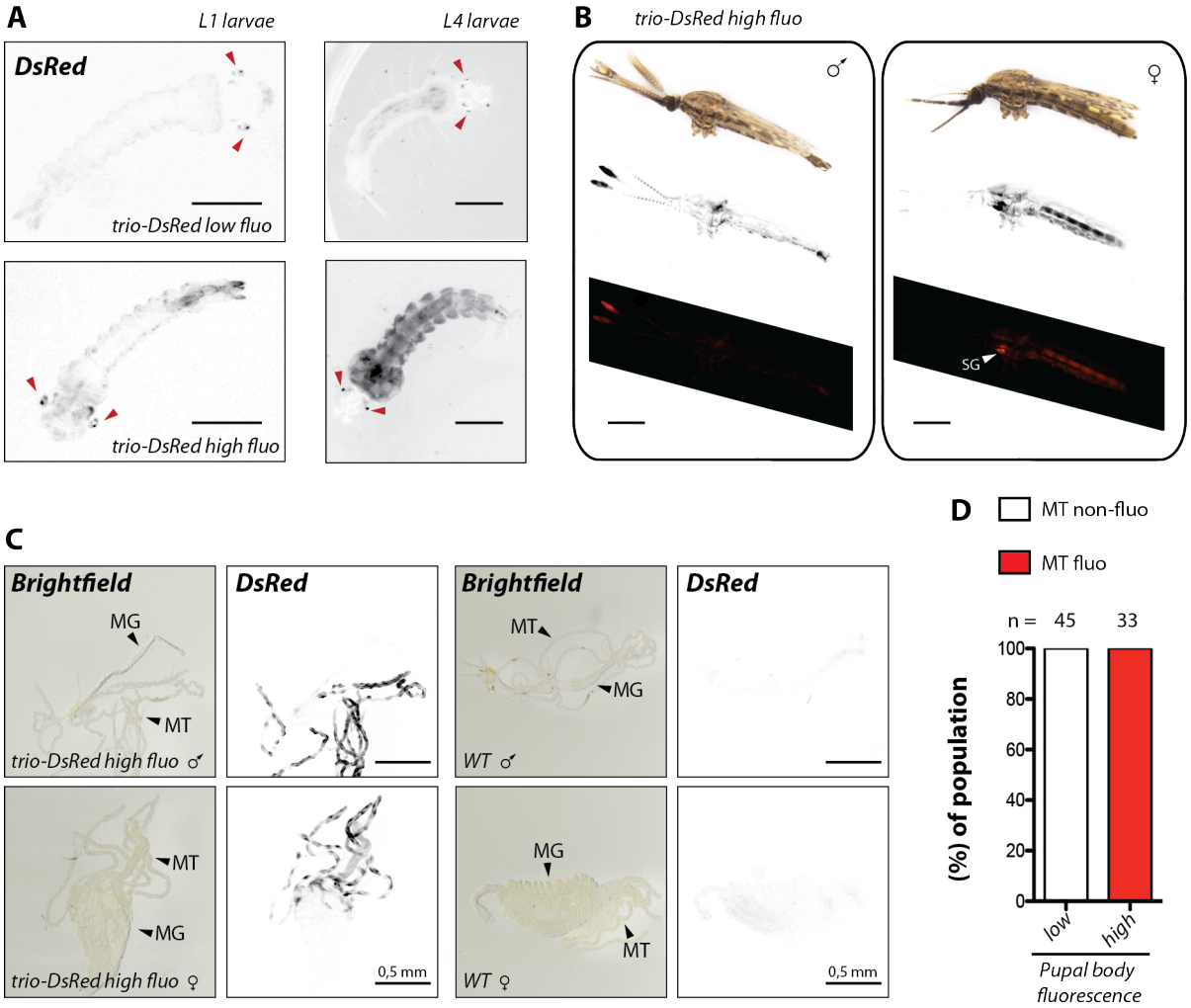

Figure S5. DsRed expression in Malphigian tubules (MT) of *trio-DsRed* mosquitoes is linked to ubiquitous DsRed expression in larvae, pupae and adults.
A) *Trio-DsRed* L1 and L4 larvae were classified as *trio-DsRed low fluo* or *trio-DsRed high fluo* according to their body DsRed fluorescence intensity. Red arrowheads point towards the DsRed positive eyes observed in the majority of larvae. Scale bar L1: 250 µm. Scale bar L4: 0.5 mm. **B)** Whole body fluorescence of *trio-DsRed high fluo* male and female mosquitoes. From top to bottom: brightfield, inverted DsRed fluorescence signal displayed in black and white and in red on black. Note that images were stitched from two separate images showing either the head or the abdominal part. Scale bar: 0.5 mm. **C)** Representative images of male and female midguts dissected from mosquitoes that displayed high body fluorescence at the pupal stage in comparison to *wild type* (WT: *G3*). Malphigian tubules (MT) and midguts (MG) are indicated by black arrows. Scale bar: 0.5 mm. **D)** Correlation of high body fluorescence at the pupal stage with DsRed expression in malphigian tubules (MT). Data were collected from two different mosquito generations. The number of analyzed mosquitoes is indicated above each column.

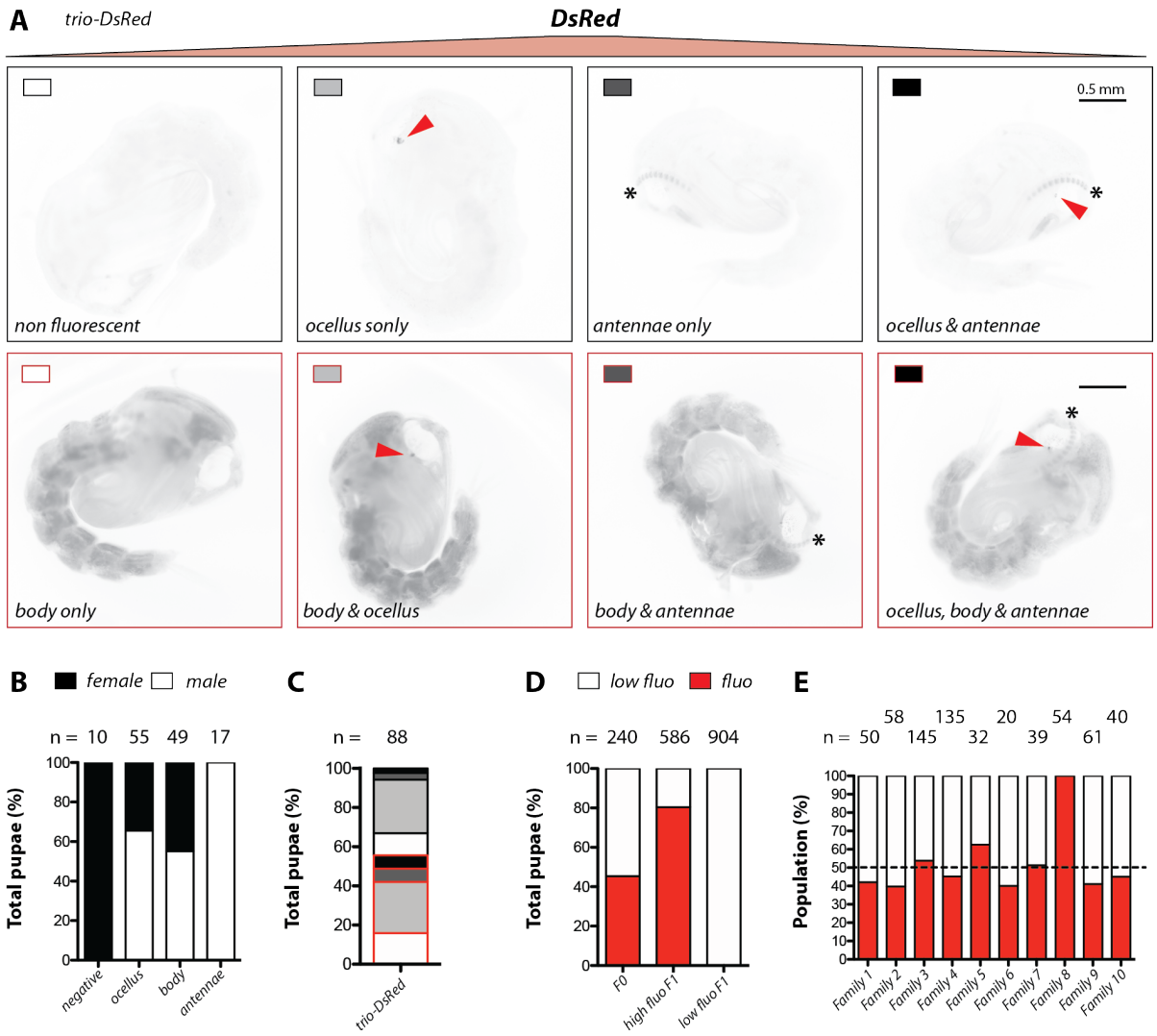

Figure S6. *trio-DsRed* pupae display high variability in DsRed expression.
A) Representative images of DsRed expression patterns in *trio-DsRed* pupae. A subpopulation of pupae displayed high body DsRed expression (images in red frames) while remaining pupae showed no DsRed body expression (black frames). Some pupae displayed fluorescent ocelli and/or fluorescent antennae. The presence of DsRed expression in body, ocelli and antennae occurred in different combinations that are represented by rectangles with different shades and frames. Scale bar: 0.5 mm **B)** Fluorescence patterns in pupae in relation to their sex. Non-fluorescent pupae were exclusively female while pupae with fluorescent antennae were exclusively male. Data pooled from four generations (≥20 pupae per generation). **C)** Proportion of each fluorescence pattern in relation to the whole population. Shading and framing of the different patterns as in (A). **D)** Proportion of pupae with high and low body fluorescence in the *trio-DsRed* colony (F0) and after intercrossing individuals displaying high or low pupal body fluorescence (F1). The number of analyzed individuals is given above each column. **E)** Females hatched from pupae with high body fluorescence analyzed in (D, high fluo F1) were kept separately and crossed to wild type males (*Ngousso*). The progeny of single females was evaluated at the pupal stage for body fluorescence (same color code as D, dashed line indicates 50% of the population). Females of families 5, 6, 7, 8 and 10 were also evaluated for salivary gland fluorescence which was present in all specimens.

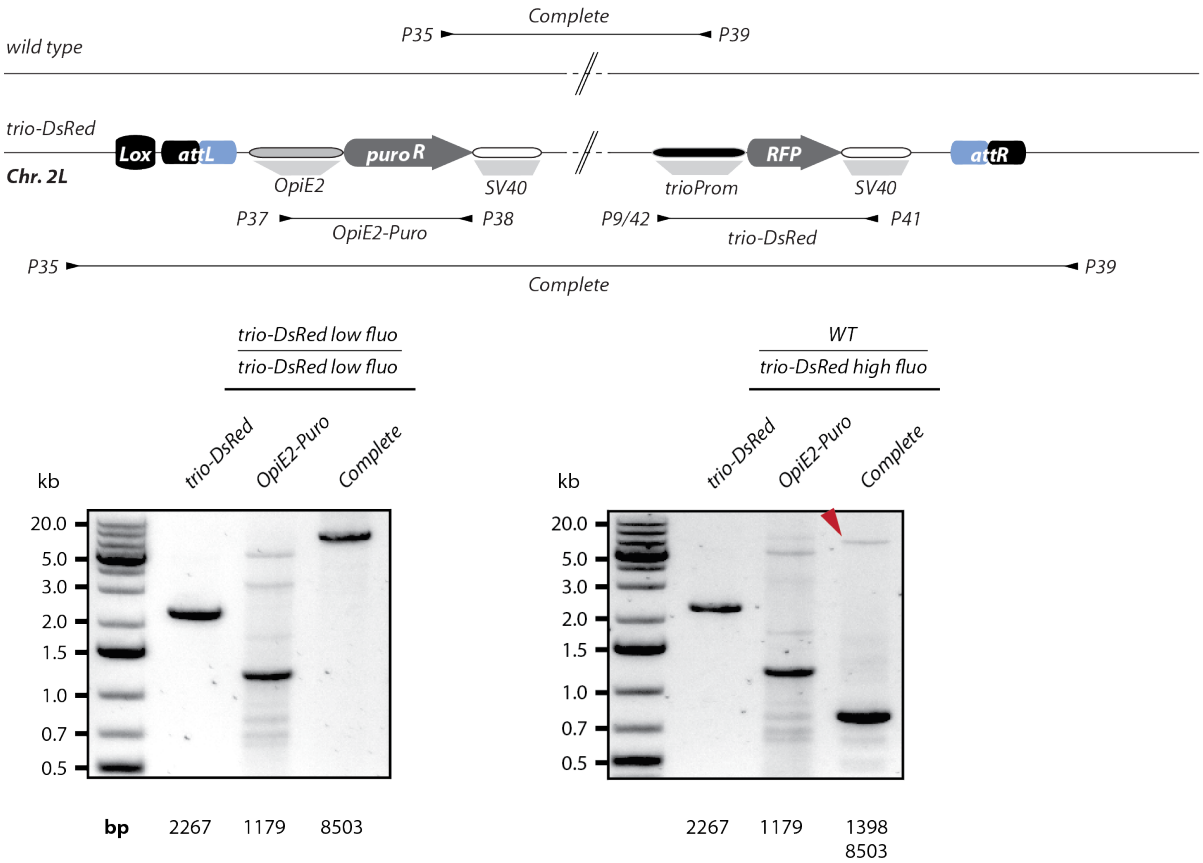

Figure S7. Genotyping of *trio-DsRed high fluo* in comparison to *trio-DsRed low fluo*. Genotyping of a female mosquito homozygous for the *trio-DsRed* low fluorescence transgene taken from the colony generated by crossing fluorescence negative pupae (see **Fig. S6D)** in comparison to a female mosquito heterozygous for the *trio-DsRed* high fluorescence transgene and the wild type allele obtained from family 1. An illustration of the modified X1 locus containing the *trio-DsRed* transgene in comparison to the unmodified wild type allele is shown on top. Genotyping primers and expected products are shown as black arrows and lines, respectively. The length of the expected PCR products is indicated below the gel images. Note that for the heterozygous female carrying the *trio-DsRed* high fluorescence transgene the smaller PCR fragment amplifying the unmodified locus dominates while the long PCR fragment representing the transgene containing allele is visible as a faint band at the upper edge (marked by a red arrow). The OpiE2-Puro PCR to verify the presence of the transgene gave several unspecific bands. PCRs were performed on genomic DNA obtained from single mosquitoes.

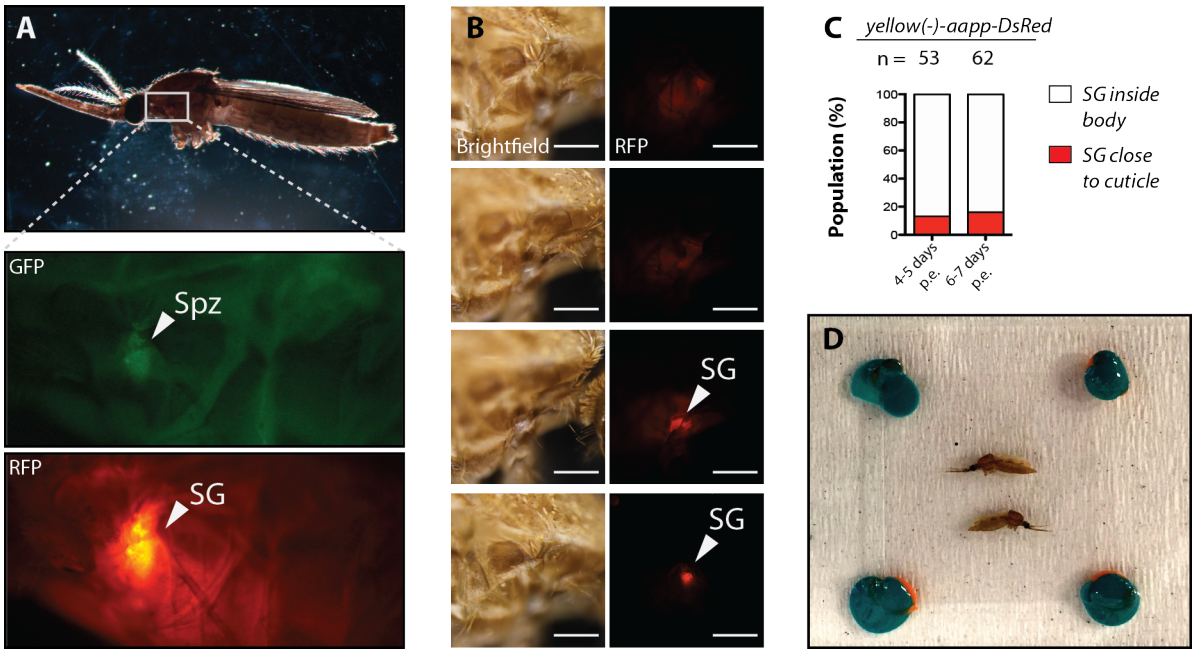

Figure S8. Selection and sample preparation of mosquitoes for *in vivo* imaging. **A)** Images of an infected mosquito with sporozoites (Spz, GFP channel) inside salivary glands and salivary gland (SG, red channel) localization close to the cuticle. GFP and DsRed images show the mosquito neck region squared in the brightfield image (top). **B)** Positioning of the salivary gland varies between mosquitoes, either deep (rows 1 & 2) or close to the cuticle (rows 3 & 4). Brightfield (left) and DsRed (right) images of the same field of view. Images were acquired with the same settings. Scale bar: 250 µm. **C)** Quantification of salivary gland positioning according to the fluorescence pattern shown in (B). Two mosquito batches were evaluated per time point post emergence (p.e.). The number of evaluated mosquitoes is indicated above each column. **D)** Sample preparation before imaging. Legless mosquitoes were glued on a microscopy slide and covered with a cover slip underlaid with orange plasticine to avoid squeezing. Corner areas were subsequently coated with teal-colored nail polish to prevent the cover slip from moving.

Movie 1. Sporozoites display active motility inside the mosquito.
Movie showing three sporozoites imaged in close proximity to the salivary gland. Sporozoites appear to be attached to a larger vessel and observed movements might be a mixture of active motility influenced by passive hemolymph flow. Imaging performed with a Hamamatsu Orca Flash 4.0 V1 camera using a 63x (NA 1.4) objective. GFP signal of a 3 min movie with 3 seconds between frames.

Movie 2. Sporozoites form accumulations close to the salivary gland.
Movie showing an accumulation of sporozoites close to the salivary gland directly below the cuticle. Several sporozoites display active back and forth movements. Imaging was performed with a Yokogawa CSU X-1 camera using a 63x (NA 1.4) objective. The left side of the movie displays the DsRed signal (salivary gland) while the right side shows the GFP signal (sporozoites) in black on white. Two min movie with 2 seconds between frames.

Movie 3. Sporozoite crawls through tissue by employing back and forth gliding.
Movie showing an actively moving sporozoite below the cuticle. The sporozoite was captured in proximity to the gland. By actively moving back and forth the sporozoite crawls slowly forward reaching eventually deeper tissues layers. Imaging was performed with a Yokogawa CSU X-1 camera using a 63x (NA 1.4) objective. The left side of the movie displays the DsRed signal (salivary gland) while the right side shows the GFP signal (sporozoites) in black on white. Two min movie with 2 seconds between frames.

Supplementary Table S1.

List of primers used for cloning plasmids to generate salivary gland reporter lines as well as *yellow(-)KI* and *sag(-)KI* lines. Nucleotides highlighted in green represent the cutting site for *Bsa*I. The guanin written in white on a black background indicates an undefined position of the *Bsa*I cutting site which can be any nucleotide. The nucleotides marked in red represent the overhangs needed for assembly of the GoldenGate building blocks. Sequences written in black define primer binding sites and nucleotides highlighted in orange represent overhangs to allow fusion of DNA sequences by assembly PCR.

Primer	Sequence (5' to 3')	Description
P1	GGTCTCGATCCCTTTTCTTTTACCCTTTGTAACACGCTAATAACG	aapp_5'UTR_forward
P2	GGTCTCGCTCTGTCGTTTTTTTGTTGTTGTGGTATTATTTCACTG	aapp_5'UTR_reverse
P3	GGTCTCGAGAGATGGCTCAAGAGTTTGTGAACTGCAAAATC	hGrx1-roGFP2_forward
P4	GGTCTCGAAGCTTACTTGTACAGCTCGTCCATGCCG	hGrx1-roGFP2_reverse
P5	GGTCTCGAGAGATGGTGCGCTCCTCCAAGAACG	DsRed_aapp/trio_forward
P6	GGTCTCGAAGCCTACAGGAACAGGTGGTGGCGGC	DsRed_aapp/trio_reverse
P7	GGTCTCGATCCTTTTCTGAGGTGATCTTTCGAAAAGATCG	trio_5'UTR_forward
P8	GGTCTCGCTCTGTAACTGGGAGCAGATTGATTTTATGG	trio_5'UTR_reverse
P9	GGTCTCGATCCCTTTCATGCGTACAATGTGTATGATCACTG	saglin_5'UTR_forward
P10	CGTTCTTGGAGGAGCGCACCATTTATAAGTGAACCTTATGCAAACCTTCCCTG	saglin_5'UTR_reverse

1072 1073	**P11**	CAGGGAAGGTTTGCATAAGGTTCACTTATA AATGGTGCGCTCCTCCAAGAACG	DsRed_saglin_forward
1074 1075	**P12**	GGTCTCGAAGCCTACAGGAACAGGTGGTGG CGG	DsRed_saglin_reverse
1076	**P13**	CCTTGTAGCGTGCCTGGTGGCCGC	Yellow_gRNA1_fw
1077	**P14**	AAACGCGGCCACCAGGCACGCTAC	Yellow_gRNA1_rev
1078	**P15**	CCTTGGCGACTACGTGCCCACGAA	Yellow_gRNA2_fw
1079	**P16**	AAACTTCGTGGGCACGTAGTCGCC	Yellow_gRNA2_rev
1080	**P17**	CCTTGGAGAACAAGCTGTTCGTCT	Yellow_gRNA3_fw
1081	**P18**	AAACAGACGAACAGCTTGTTCTCC	Yellow_gRNA3_rev
1082	**P19**	GGTCTCGAACAGAATTGAACGCCCAAGGTACGGCTG	Yellow_5’UTR_fw
1083	**P20**	GGTCTCACCCCGCTTCTGCCACTAAGGAACTTCTGTG	Yellow_5’UTR_rev
1084	**P21**	GGTCTCGAAGACGTGTGTCCTGGAAGTGTGATTTATCG	Yellow_3’UTR_fw
1085 1086	**P22**	GGTCTCGAAGCGTAGCGTGCCTGGTGGCCGCCGG AACGCTTTCCCTGCAGCGTAC	Yellow_3’UTR_rev
1087	**P23**	CCTTGCGTTCAAGTCATCTCGAGC	Saglin_gRNA1_fw
1088	**P24**	AAACGCTCGAGATGACTTGAACGC	Saglin_gRNA1_rev
1089	**P25**	CCTTGCCGCAGTCCTCGCGGCTGG	Saglin_gRNA2_fw
1090	**P26**	AAACCCAGCCGCGAGGACTGCGGC	Saglin_gRNA2_rev
1091	**P27**	CCTTGAAGTTTGCAACGTTTGCGA	Saglin_gRNA3_fw
1092	**P28**	AAACTCGCAAACGTTGCAAACTTC	Saglin_gRNA3_rev
1093	**P29**	GGTCTCGAACATGGGTTCACTCGCTGTTAGACTGTG	Saglin_5’UTR_fw

P30	GGTCTCAATGGTTATAAGTGAACCTTATGCAAACCTTCCCTG	Saglin_5'UTR_rev
P31	GGTCTCGAAGAGCGTCGGCGACGGTCTAAAAG	Saglin_3'UTR_fw
P32	GGTCTCGAAGCGTTCAAGTCATCTCGAGCCGG CTTCTTCTGCTGCCGCAGAAAC	Saglin_3'UTR_rev

1099 **Supplementary Table S2.**

1100 List of primers used for genotyping. Note that some primers used for construct cloning have
1101 also been used for analytical PCRs.
1102

Primer	Sequence (5' to 3')	Binding site
P33	GGTCTCGAACAGAATTGAACGCCCAAGGTACGGCTG	yellow_5'_forward
P34	GGTCTCACCCCGCTTCTGCCACTAAGGAACTTCTGTG	yellow_5'_reverse
P35	CCCGTCATGAGTTCAAGCCTGAA	X1_forward_1
P36	CCCGGTCTCAAATTGCCCGCCGTGACCGTCGA	attB_reverse
P37	CAAGCACCTTTATACTCGGTGGCCTC	OpiE2_forward
P38	TTCCAGGAAGGCGGGCACCCC	PuroR_reverse_1
P39	ACTGCAACCCATTCACACTG	X1_reverse
P40	CAGGGAAGGTTTGCATAAGGTTCACTTATAAATGGTGCGCTCCTCCAAGAACG	DsRed_forward
P41	CCTCTACAAATGTGGTATGGCTGA	SV40_reverse
P42	GGTCTCGATCCCTTTCATGCGTACAATGTGTATGATCACTG	sag_forward
P43	CCTTGAAGATTGGAATCCATCCAT	X1_forward_2
P44	GGTCTCGATCCCTTTTCTTTTACCCTTTGTAACACGCTAATAACG	aapp_forward
P45	GGTCTCGATCCTTTTCTGAGGTGATCTTTCGAAAAGATCG	trio_forward
P46	GGTCTCGAGAGATGGCTCAAGAGTTTGTGAACTGCAAAATC	hGrX1-roGFP2_forward
P47	GCTTATAAGAGCGCTACGGGTGTAC	Sag_5'_fw_genotyping
P48	CTGTCCCTTCAGCTTCACCAGCTC	Sag_3'_rev_genotyping
P49	GAACGACAGGTGAGCTGACAGTAAC	Yellow_5'_fw_genotyping

P50	GATTTGGCGAGATGGTTTGTGCGAC	Yellow_3’_rev_genotyping
P51	GAGCTCGAGTTCAGGCACCGGGCTTGC	PuroR_reverse_2
P52	CTTCGGGCATGGCGGACTTG	EGFP_reverse
P53	CAGCCATACCACATTTGTAGAG	SV40_forward

Supplementary File S1.

Promoter sequences of the *trio*, *saglin* and *aapp* genes used to generate the mosquito lines *aapp-DsRed*, *aapp-hGrx1-roGFP2*, *sag-DsRed* and *trio-DsRed*. Nucleotides highlighted in red are part of the primer sequence used to amplify the promoter sequence. Sequences with a grey background indicate the 5'UTRs of the *trio* and *aapp* transcript, respectively.

***aapp* promoter sequence (AGAP009974, 1673 bp):**

```
      CTTTTCTTTTACCCTTTGTAACACGCTAATAACGAAAGACCTCCTGCGTGTTAGTACG
TGGTGAGGATGATGCGTTTTAGCCTAGCTAGTATTCAAAAAACCTATTAATGCAACAATTAC
AGTGTGAGGTTACAAAATGGAATTAATTAAACACACTGCTCAACACAGCCATCGTGCTGCAT
CGTGCTTTGTTGAGGCGCAACAGTTAAATTGTAAGTGCAACCACCGGTATAGAGAGCTGCTT
TTGGCAAATGATATGGAATTGTGCTAAATTATGTAATGTTTTTTTTAACTAACTCGTTTACC
CGTTAATGGTGGAATGTTTGCAGGTGCGTAGATTAATTTTTTTTAAATGTGCAAATGGAGAA
AACAGGATAACGCAAAAGTATTTCCTTCGCTGTAGTAATAGGCTATTATTTATGTACGTCTT
TATGTGACCCCGCTAGTGTTGGCTGTATTTTATATCTGTAGGTAAATGACGCGCTATGTATT
GTAATAAAATTGGACAAACATTTGCATGTACGATCTGTTAGCTTAGAGAATAAGTATTTTTC
TTTTTCGCTACATTTCTCTAAATTCGACCGACGATGACTGTTTTAGGTGTTTTTTCGTAACT
TGATCAAGGTAACACCTTTTCTTGGCGTAACGTCCTACGCGGACATGCCGGCCGGCCTTATT
CAGGCTTTCGAGACTTAATTCATTACCACGTAGCCGGATAAGTCCAATCCTTGCACAACGGG
GGAACGGGTGTCCATTTCAGGCTTGGGCCCATGACGGGCATGTTATTGAGTCGTTCGAGTTG
ACGACTGTACCATGGGACCGCCCCATTTTTGGCAGTCCATTGATCGTTACGTCGTTTTACGT
CTACTGAAGGATGTCCGTTATCAGGTCAAGTCCAGCATAGATTAAGTCTCCCATACGAAGGA
TTGATTAGCTCGAGACTTAATGTTATATACAAAATTCTTATACATGTTCTAGATCAGGATTG
TTGCGCTACACTGTCTTCCATGTCGATCTTCTATATTCAGTTTTTGGCACAGTGATCGTCAC
TGTAATCTCAATAGATTTGAATTTCAATACTTCTATGGGAGGAGGATGAGTAGAAAGGTGTC
CAAAGCGCTGGATCTATGGCTGCAACTCCTCATGCTTGTAAGCACCCGACAGCCAATTCGAT
CTACCTGACCTGATGCGGTATTCGAACTAAAAGCACAGATCAAGCACTGTTTCACACGATCT
GAAGCACTGTTCTACTGCAAAGATAAGTGCATATTAGTTATTTTTCATACCGATCTTCACTG
CGACGGTTTAGCGATCTTCATTATTTTCCACCTTCACCCCTCAACCCAGGGAGTGCGCTTTT
CCCCGTCGAGATAAAATTACTAAATGTAAACTTTGCATGCAATTATGTAGCTGTATGGTAAG
CAAATAAAAATCTTTCCTCCTATTGCAACACGTCGCTTGTTTGCAGCGGATATTTGCCCACA
GTAAAGCCCGATCGCCTGTGCATTGTGTTTAACACGTGCTGCAAGCTGTATCAATACCGATC
GATTGTATGATTCCACGATCTTCGTGTGGTATAAAAACGGCGCTGAACAGCAGTAAAGATCA
TCACTTACATTTGTTTTATTCTCCACGGAGTCAGTGAAATAATACCACAACAACAAAAAAAC
G
```

***trio* promoter sequence (AGAP001374, 1537 bp):**

TTTTCTGAGGTGATCTTTCGAAAAGATCGATCGACCGACCCCCAACGGCAACTCTCCC
TCGGATGACCTCAGCCCAGAATAGGCATTCTTTCAGCAAGTCATTCTATCATCCCTTTTACA
TCTTACGTTACTCCAAAAAAAGAGAAGCTTTCCACCCCAAAGCTTTCGTTGTGGTGCAGCTT
TCGATGGTGATCGCGATCACGGTACCACACGTACGTTTGTTTGCTACTCTCGCTCACCGTTT
TCTTCGATTTCGTGTCTCGGGTACCGTTTGCTCGGTGCGGTAGTGCTGCGAAGAAAGCCGTT
GGCCGAGAGAATAATGCTCACTTCGGCTGCACGCAACTCGCCGTGCCACAGCCGTGGAAGGG
GTAGGTTGGATGGTCGGGGTCGGGACCGCAACGCCGAAGTGAACGCCGGCGTGCCAGCGAAC
GATCGCACCCCGGCACAGTCCAACTGCGTCGCTGGGCGCGCTCGGCGGACGGTTCTCGGTGT
GTGCGCCCCCTTTGGTGCTCATCCCTCATATCTCATCTCATCCTTTCGCGCTGCTCGCGGTT
CCCGCAGAACCACGCGCGAGAGGGAGTTGCGCGAACCAGGGAGAGCCCGACACCTGGGCAGC
GTCCAGGCGGACCTGTTCGGGAACGGTCGCGGTGTATAAAACTCGATTCCCGCCCGCCGTTA
GGTAACAGTCCATTGTGTAACGTTGCCGGGATCGCGAGCCATCCTGCAGGAACACAGCCGTG
CGAGTTTGTGTGCGCGTGTATTTTGCCTACAAGCAAGTGAGCAGCAATCAGTGAGAACAACA
TCTAAAACAGAAAAACAAACAGTGAACTACAGTGCTGTGGAGCAGTGGAAATTGGTGTTAAT
TGAAGAGCTTTGTACATCGATCACACGGACAACCACGCACGTGGAGAAAGTTCTGCTGCGGT
GCGGGTTACTTGCGTACACCACATTAAACATTGTGTGTGGCATTTAAAATAAATATACTCGC
GCCCTCCCCTCAGCTGCTCTCGCGGGCACGCCCGATGCCAGAGGTCGCCCCGACCGGACATT
GAACGTGGAAAGAAGAAAGTTGTCGGTTGTTTACACTTCCGTCCTGAGTGGTGTTGTGGCTA
CCGTTTGTGACCGTTGGTGAAATAAAGTAACATACCCCTCCCGAGGGCAGCAGCGACAATGA
CCTCCGGAAATTCGATAACAATACGTAAGTTACTTTCATTTTTTGCAAATTAAATTACCTCG
TGATAATTGAGTGGAGTGAGTAGGTACAGGTTGTTAACGCGTCTTTTGTTTAGTTCGGCAAT
CCGGATCCGAAGATGAGAGGAGATTGCCTCTGATGATGATGTTATCATGATTGCTTGTGTAA
CGACGCAAAGATTCTCAGAGAACAACTTCTCCCAACATAATTAATCTTGTTGAAGGGTCTGT
AAACACGTGGTGGGATATCTTACAACTGAACCAATATTCGACCGATAGTATAAAGTCCTTCG
CACCATCGATGCGTTTACCATTTTCCCATAAAATCAATCTGCTCCCAGTTACA

***sag* promoter sequence (AGAP000610, 220 bp):**

CTTTCATGCGTACAATGTGTATGATCACTGATGACAAAGCGCTTGGGTGGGCGCTTGC
TGCTGAAGCGTGGCTGACAAATGGGGGGGGGGGGGCTTGAACAAATATTTGCACACACGAT
AATGCTCTTGTTTGCCATGCGCTGACGGAAGACAAATCGCTGCAAGCGACGGCTCAAACCTG
CTCAAACCAGGGAAGGTTTGCATAAGGTTCACTTATAA